Check for updates

# Cost-effective eggshell-modified LDH composite for caffeine adsorption, cytotoxicity and antimicrobial activity: exploring the synergy and economic viability in search processes†

Asmaa Elrafey,[a] Ahmed A. Farghali,[b] W. Kamal,[c] Ahmed A. Allam,[de] Zienab E. Eldin,[b] Hassan A. Rudayni,[d] Haifa E. Alfassam,[f] Alaa A. A. Anwar,[c] Sara Saeed[c] and Rehab Mahmoud*[c]

The rise of pharmaceutical residues poses a serious threat to ecological and aquatic environments, necessitating the development of cost-effective, convenient, and recyclable adsorbents. Given the high global consumption of eggs, a significant amount of waste eggshell is produced. The techniques outlined here aim to manage eggshell waste by transforming it into highly valuable products, addressing the issue of eggshell waste in communities and industries. This approach supports the concept of zero-waste operations to create value-added goods, contributing to sustainable development. In the future, this method of waste management and material recycling may be adopted as an alternative. CaO-based ZnFe-layered double hydroxide (LDH) is identified as an efficient adsorbent for caffeine (COF) residues due to its biodegradability and biocompatibility. We extensively analyzed the synthesized CaO, ZnFe-LDH, and CaO/ZnFe-LDH composites before the adsorption processes using FT-IR, XRD, SEM, EDX, BET surface area, PZC, TGA/DTG, and after the adsorption processes using FT-IR. We investigated factors affecting the adsorption process, such as pH, adsorbent dose, COF concentrations, and time. Six non-linear adsorption isotherm models were studied at pH 7 for the composite and pH 9 for LDH, showing maximum adsorption capacities ($q_{max}$) of 152.35 mg g$^{-1}$ for LDH and 194.87 mg g$^{-1}$ for CaO/ZnFe-LDH. Kinetic studies were also conducted. Interestingly, the MTT assay conducted on WI-38 cells revealed minimal toxicity, with most tests indicating cell viability above 60%. The synthesized CaO, ZnFe-LDH, and CaO/ZnFe-LDH composite exhibit robust antimicrobial properties against two pathogens, including Gram-negative bacteria (*Escherichia coli*) and Gram-positive bacteria (*MRSA*). The MIC values for the synthesized materials range from 0.87 to 7 μg mL$^{-1}$, varying with the microbial species. Two green metrics were applied: the analytical Eco-scale and the Analytical GREEnness Calculator (AGREE).

*aEnvironmental Science and Industrial Development Department, Faculty of Postgraduate Studies for Advanced Sciences, Beni-Suef University, Beni-Suef, Egypt. E-mail: Asmaa_elrafey@hotmail.com*

*bMaterials Science and Nanotechnology Department, Faculty of Postgraduate Studies for Advanced Science (PSAS), Beni-Suef University, Beni-Suef 62511, Egypt. E-mail: Ahmedfarghali74@yahoo.com; t-zienabessam@zewailcity.edu.eg*

*cChemistry Department, Faculty of Science, Beni-Suef University, Beni-Suef 62511, Egypt. E-mail: rehabkhaled@science.bsu.edu.eg; Sarasaeedabdelazeem@gmail.com; Wesamkamal16@yahoo.com*

*dDepartment of Biology, College of Science, Imam Mohammad Ibn Saud Islamic University, Riyadh 11623, Saudi Arabia. E-mail: HARUDAYNI@imamu.edu.sa*

*eDepartment of Zoology, Faculty of Science, Beni-Suef University, Beni-Suef 65211, Egypt. E-mail: Ahmed.aliahmed@science.bsu.edu.eg*

*fDepartment of Biology, College of Science, Princess Nourah bint Abdulrahman University, P. O. Box 84428, Riyadh 11671, Saudi Arabia. E-mail: halfassam@pnu.edu.sa*

† Electronic supplementary information (ESI) available. See DOI: https://doi.org/10.1039/d4ra04558k

## 1 Introduction

Among the most exciting emerging pollutants are pharmaceutical compounds, which have been found in aquatic media at concentrations ranging from nanograms per liter to milligrams per liter.

The primary causes of these pollutants' presence in the environment are anthropogenic activities, which primarily involve animal activity, municipal wastewater treatment facilities, and hospital effluents.[1] COF is one of the weak alkaloids in the methylxanthine family, specifically 1,3,7-trimethylxanthine. Since this substance boosts the nervous system and causes momentary variations in heart rate, it is regarded as a drug. While excessive COF intake can lead to adverse effects—such as difficulty sleeping, an increased risk of cardiovascular disorders, decreased fertility, and an increased risk of miscarriages. It is commonly used as a diuretic drug.[2] COF acts as an adjuvant
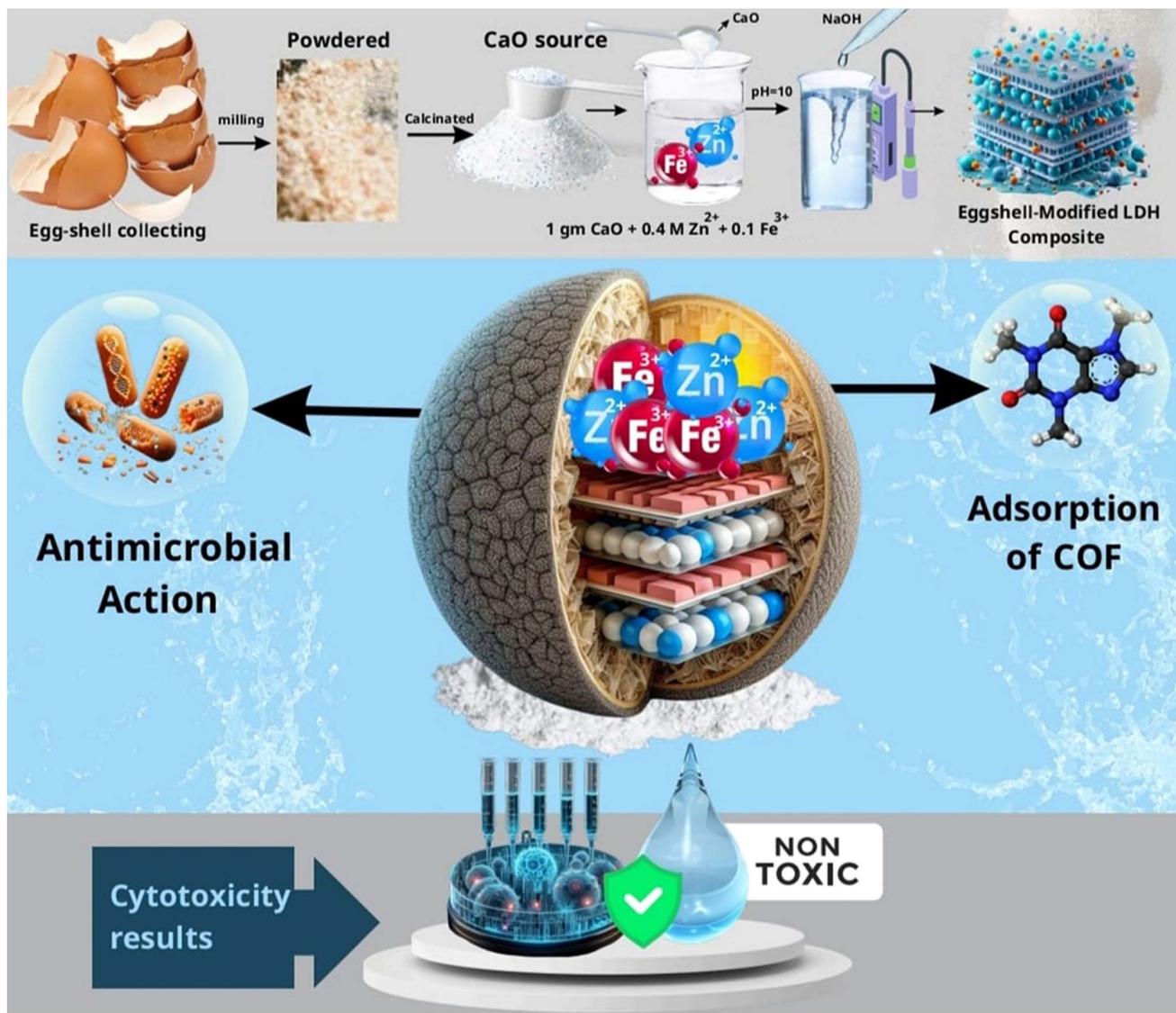
Scheme 1 Diagram eggshell-modified LDH composite for COF adsorption and antimicrobial activity.

to increase the analgesic effects of many pharmacological formulations. It can be found in many foods, such as chocolate, coffee, tea, and soft drinks. Since this substance is excreted in small amounts (1–10%) due to its rapid metabolism. Many pharmaceutical chemicals, including COF, are classified as water contaminants and are considered emerging pollutants. Since the presence of this set of toxins in the environment was only recently found, there is considerable concern for the environment. Certain academics consider COF to be an indicator of human contamination because it resists conventional water and wastewater purification methods. Consequently, it has been common to find this material in both surface and groundwater.[3]

Adsorption, complex oxidative processes, bioremediation, and membrane separation are some of the methods used to treat contaminated water. Various impurities, including COF, can be effectively removed from aqueous solutions using these techniques.[2]

Adsorption is economical, flexible, efficient, and ecologically safe. One of the many contaminants in water that can be eliminated by adsorption is COF. This is particularly useful for non-biodegradable pollutants including heavy metals and emerging contaminants (ECs). COF removal by batch and fixed bed adsorption techniques has recently been reported. Granular activated carbon (GAC) and powdered activated carbon (PAC) are commonly used adsorbents due to their favorable chemical surface properties and significant specific surface area.[4]

Various types of adsorbents can remove COF from aqueous solutions, such as raw or modified biosorbents, biochar, activated carbons, graphene nanoplatelets (GNPs), multi-walled carbon nanotubes (MWCNTs), natural clay, carbon xerogels, metal–organic frameworks (MOFs), molecularly imprinted polymers (MIPs), hydrogel beads, and chitosan and its derivatives.[1] Research aimed at eliminating COF and demonstrating encouraging results in the literature, as illustrated in Table 1, highlights the primary challenge in current adsorption

**Table 1** Previous studies in the open literature reporting adsorbents for COF removal

| Adsorbent | pH | Adsorbent mass (g L$^{-1}$) | Equilibrium time | $q_{max}$ (mg g$^{-1}$) for COF | Ref. |
|---|---|---|---|---|---|
| **ZnFe-LDH** | **9** | **0.05** | **50 min** | **152.35** | **This work** |
| **CaO/ZnFe-LDH** | **7** | **0.05** | **40 min** | **194.87** | **This work** |
| Bimetallic zero-valent iron/copper nanoparticles | 5 | 0.2 | 45 min | 34.34 | 1 |
| Activated carbon prepared from coconut leaf | 7.9 | — | 30 min | 73.83 | 2 |
| Sepiolite clay | 6 | 1.6 | 10 days | 48.7 | 3 |
| Oxidized carbon derived from *Luffa cylindrica* | 4 | 0.05 | 80 min | 59.9 | 4 |
| MgAl-LDH/biochar | 12 | 4 | 20 min | 26.2 | 5 |
| Fique bagasse biochar | 12 | 0.03 | 16 h | 40.2 | 6 |
| Activated pineapple leaf biochar | 7 | — | 4 h | 155.5 | 7 |
| Synthetic xerogel coals | 6.9 | 0.06 | 48 h | 182.5 | 8 |

research: the development of new adsorbent materials. Double lamellar hydroxides (LDHs) possess various characteristics—such as composition, thermal stability, and other physico-chemical qualities—that contribute to their diverse applications. Common applications for LDHs include their use as adsorbents, catalysts, anion exchangers, and in pharmaceuticals. LDHs exhibit promising properties as adsorbents due to their extensive surface area, high porosity, and layered structure.[5]

The preparation of LDH materials utilizing novel approaches, cutting-edge alterations, eco-friendly practices, and simple operation presents a challenge. Because of its low solubility product reach of 62.51 (ref. 9) and high stability constant of approximately 25.27, ZnFe-LDH was chosen as our model for the study over other LDHs. New recycling techniques must also be developed due to the growing volume of solid adsorbent wastes. Globally, this is an essential requirement.

Utilizing natural resources, kitchen waste, and agricultural byproducts as fillers in the production of polymer green composites is gaining popularity due to increasing environmental awareness. Improper disposal of eggshell powder (ESP), a poultry waste product, can have detrimental effects on the environment. Adding value to this poultry and kitchen waste was the goal of some studies.[10]

Because calcium carbonate (CaCO$_3$) sources and their precursors are readily available in nature, these catalysts are inexpensive, environmentally friendly, and effective at low temperatures and pressures. Additionally, they are easy to handle, exhibit low solubility, high basicity (which allows for recycling), and can be regenerated. These factors have sparked recent interest in calcium oxide (CaO)-based catalysts. Typically, the thermal decomposition of CaCO$_3$ yields CaO-based catalysts. Examples of natural calcium sources used as feedstocks to produce CaO-based catalysts include eggs and *Turbo jourdani* (Gastropoda: Turbinidae).[11]

Calcium carbonate, typically extracted from limestone sedimentary rock, is one of the most abundant biominerals on Earth, prized for its biocompatibility and cost-effectiveness in various applications. A more sustainable approach involves utilizing biogenic waste shells, such as those from poultry eggshells and seashells, as sources of calcium carbonate.[12] These waste shell biomaterials, rich in CaCO$_3$, present opportunities for producing renewable heterogeneous catalysts. Additionally, they may serve as cost-effective fillers or ingredients in the production of hydroxyapatite (HA) powder, which is commonly used as a biofilter medium in wastewater treatment. Compared to conventional materials used in wastewater treatment, cement production, and catalyst manufacturing, these biogenic materials are more sustainable, affordable, and environmentally friendly.[13] The objective of this work is to synthesize the CaO/ZnFe-LDH composite using eggshell-derived calcium oxide (CaO) as a scaffold and to evaluate its effectiveness in removing COF from aqueous solutions. To achieve this, the substance was synthesized using the co-precipitation method and analyzed through various techniques. A thorough discussion of the equilibrium and kinetics studies is provided.[5] This study synthesized and characterized CaO/ZnFe-LDH. Additionally, we investigated the capacity of the produced catalysts to remove COF from aqueous solutions at different concentrations and pH levels. Furthermore, we assessed the antibacterial activity of LDH, CaO, and CaO/ZnFe-LDH against various bacteria (Scheme 1).[14]

Green analytical chemistry aims to reduce costs for analysts, minimize hazards, and enhance environmental sustainability.

Key components of green analytical chemistry include reduced solvent usage, the utilization of low-toxic and environmentally friendly compounds, shorter analysis times, lower energy consumption, and improved integration, disassembly, and user-friendliness of instruments and protocols.[15] Green chemistry metrics elucidate chemical reactions that adhere to green chemistry principles. These metrics serve to monitor performance improvements and evaluate chemical process efficiency and environmental impact.[16]

Recently, several green metrics have been developed to assess the alignment of analytical procedures with the principles of green analytical chemistry. The National Environmental Metric Index (NEMI) serves as a qualitative tool. Although the analytical method known as AGREE (Analytical GREEnness

Metric Approach and Software)[17] is quantitative, the green analytical procedure index GAPI[18,19] is semi-quantitative.

## 2 Experimental

### 2.1. Chemicals

[$C_{16}H_{15}N_5O_7S_2$, 98.5%] COF anhydrous (1,3,7-trimethylxanthine) (purity 98.5%) was bought from Arshine Pharmaceutical Co., Limited in China. The ferric nitrate ($Fe(NO_3)_3 \cdot 9H_2O$) (purity 98%) and zinc nitrate ($Zn (NO_3)_2 \cdot 6H_2O$) (purity 98%), which were bought from Alpha Chemika, were utilised to make an adsorbent LDH. Hydrochloric acid (HCl) (ACS BASIC Scharlau) (purity 37%, Piochem), sodium hydroxide (NaOH) (purity 99.8%, Sigma-Aldrich) and ethanol ($CH_3CH_2OH$) (purity 99.9%, bought from Piochem) were utilized.

### 2.2. Preparations of the adsorbents

**2.2.1. Preparation of CaO.** Eggshell waste was obtained from cake shops, bakeries, and commercial food facilities in Beni Suef, Egypt. High-purity calcium oxide was produced by processing the eggshells using the following procedure: they were cleaned with dish soap, then crushed. After several rounds of washing with bi-distilled water, the eggshells were dried in an oven set at 100 °C for a whole day. The leftover eggshell material was ground into a powder and sieved through a 50 mesh screen using a grinder machine and a 0.08 mm sieve wire. Following that, they were calcined at 900 °C for five hours in a furnace[11] (Fig. 1(a)).

**2.2.2. Preparation of ZnFe-LDH adsorbent.** An aqueous solution was prepared by co-precipitation with continuous stirring, containing 0.4 M $Zn^{2+}$ and 0.1 M $Fe^{3+}$. Next, using a titration device and constant stirring, a 0.5 M NaOH solution was added at a rate of 1 mL min$^{-1}$ until the pH reached 10.0. After a 24 hour aging period at 70 °C, the precipitate formed. The solution was then centrifuged to extract the precipitate, and the pH was adjusted to 7 by repeatedly washing it with distilled water. Finally, after a 24 hour oven drying period at 50 °C, the precipitate was mixed with ethanol (Fig. 1(b)).

**2.2.3. Preparation of CaO/ZnFe-LDH adsorbent.** Using the co-precipitation approach, which has been explained in detail in the previous section, one gram of CaO was suspended in a 250 mL beaker containing 100 mL of an aqueous solution with 0.4 M $Zn^{2+}$ and 0.1 M $Fe^{3+}$ (Fig. 1(c)).

### 2.3. Materials characterization

A variety of instruments were used to characterize the prepared substance. Utilizing Cu-Kα radiation, a Panalytical (Empyrean) X-ray diffractometer was employed to determine the crystallinity and structural makeup of the generated materials. Operating at a voltage of 40 kV and a current of 35 mA, the diffractometer scanned at a rate of 8° per minute from 5° to 80° (2θ). The infrared spectra of the produced substance were captured in the 4000–400 cm$^{-1}$ wave number region using a Bruker-Vertex 70 spectrometer. This was done after homogenizing 0.50 mg of each material with 300 mg of optically high-purity KBr and applying a 15 minute pressure to the mixture under 10 t cm$^{-2}$.

The microstructure and morphology of the synthesized adsorbents were examined using a scanning electron microscope (SEM). Energy dispersive spectroscopy (EDX) (performed with a Quanta FEG250 Instrument from Germany) was used to evaluate the elemental composition of the nanocomposite $N_2$ adsorption was employed to determine the BET specific pore volume, specific surface area, and pore size distribution of the nano-adsorbents. This analysis was conducted using an automated surface analyzer (TriStar II 3020) from Micromeritics in the USA. Thermogravimetric Analysis (TGA) was carried out using a Shimadzu DTG-60H instrument from Japan. The material (approximately 8 mg) was heated from 0 to 500 °C at a rate of 10 °C min$^{-1}$ under a nitrogen flow of 40 mL min$^{-1}$.

### 2.4. Adsorption study

The ZnFe-LDH and CaO/ZnFe-LDH solutions were shaken with a 20 mL water sample containing 20 mg L$^{-1}$ of COF. Adsorption tests were conducted at room temperature (200 rpm) using an orbital shaker. The ideal adsorption conditions were investigated by varying solution pH (ranging from 3 to 9), initial COF concentration (ranging from 5 to 100 mg L$^{-1}$), adsorbent dose (0.01 to 0.10 g), and contact period (1 to 24 hours). After each experiment, the solution was filtered to remove the adsorbents. COF concentration was measured at 273 nm using a UV-visible spectrophotometer (UV-2600, Shimadzu, Tokyo, Japan).[14] The COF adsorption efficiency for both ZnFe-LDH and CaO/ZnFe-LDH can be calculated using an appropriate equation:

$$R\% = \frac{C_o - C_t}{C_o} \times 100 \tag{1}$$

The variables $Q$, $C_o$, and $C_t$ represent the adsorptivity (%), initial concentration (%), and concentration (mg L$^{-1}$) of COF following adsorption at time $t$ (minutes). The amount of COF adsorption at equilibrium ($q_e$, in mg g$^{-1}$) can be determined using the equation:

$$Q_e = \frac{(C_o - C_t) \times V}{m} \tag{2}$$

The equilibrium adsorption capacity of the adsorbent, expressed in mg (pollutant)/g (adsorbent), is denoted by $q_e$. The starting concentration of COF before adsorption is given by $C_o$ in mg L$^{-1}$. $C_e$ represents the COF equilibrium concentration, measured in milligrams per liter. $m$ stands for the adsorbent's weight in grams, and $V$ is the COF solution's volume in liters.

To determine the adsorption isotherms of LDH, various initial concentrations of COF were applied to optimized ZnFe-LDH and CaO/ZnFe-LDH. To evaluate the adsorption rate and the time required for ZnFe-LDH and CaO/ZnFe-LDH to reach equilibrium, adsorption kinetics experiments were conducted. Specifically, 0.05 g of each adsorbent, ZnFe-LDH and CaO/ZnFe-LDH, were added to 20 mL of COF solution with an initial concentration of 50 ppm. The solution was agitated at 300 rpm at room temperature for 200 minutes, and samples were collected at predetermined intervals for analysis.
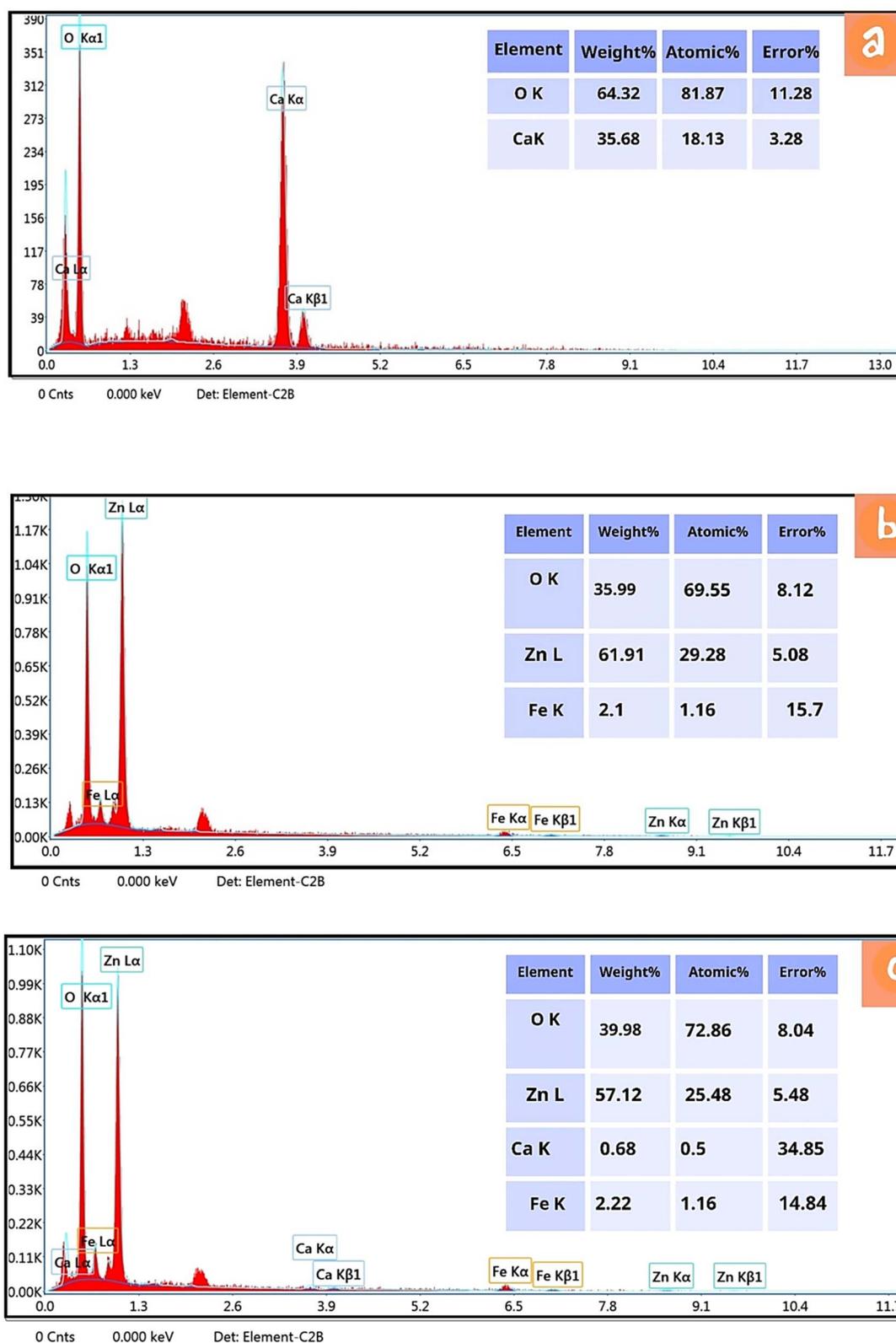
Fig. 1  EDX of (a) CaO, (b) ZnFe-LDH, (c) CaO/ZnF-LDH.

In the regeneration tests, DMF, isopropanol, and methanol were used as adsorbent reagents. Twenty milliliters of each adsorbent reagent were mixed with 0.05 grams of waste adsorbent. The samples were then shaken for 24 hours at 25 °C and 120 rpm. Desorption equilibrium capacity was determined by measuring the amounts of COF using ultraviolet-visible

spectrophotometry. The regenerated adsorbent was subsequently used in adsorption tests to assess the adsorption efficiency of each adsorbate during each repeated use.

Real sample treatment was conducted on three different water samples: tap water, River Nile water, and wastewater. Each sample was initially spiked with 5 ppm of COF, and the pH was adjusted as needed. The removal process was then performed using an optimal dose of 0.05 g of either ZnFe-LDH or CaO/ZnFe-LDH, with the process running for three hours.

### 2.5. *In vitro* cytotoxicity study

**2.5.1. Cell culture.** The Holding Company for Biological Products and Vaccines (VACSERA) in Egypt produced the normal human lung fibroblast cell line WI-38. We cultivated WI-38 cells in DMEM medium. Both were kept in an incubator with 5% $CO_2$ at 37 °C and supplemented with 10% fetal bovine serum. Trypsin–EDTA, Trypan blue dye, MTT reagent, and DMSO were used to separate the cell once it reached confluency.

**2.5.2. MTT assay.** The cell line WI-38 was seeded at a density of $2 \times 10^6$ cells per well onto 96 well plates. The cells were treated with different quantities of ZnFe-LDH, CaO, and CaO/ZnFe-LDH nanoparticles, ranging from 500 to 1 μg mL$^{-1}$, after being given a day to attach. The only treatment given to control cells was the DMSO vehicle. The prepared samples were allowed to sit for 48 hours before the MTT reagent was added and each well was incubated for a further two hours. A TECAN Sunrise microplate reader was used to measure the optical density at 590 nm after the formazan crystals were dissolved in DMSO. Eqn (3) was used to determine the cell viability percentage:

$$\text{Viability (\%)} = [1 - (OD_t/OD_c)] \times 100 \tag{3}$$

where $OD_c$ is the mean OD of the untreated control wells and $OD_t$ is the mean OD of the wells treated with LDH.

### 2.6. Bacterial strains and culture conditions

Two pathogenic bacterial strains were obtained for evaluating antibacterial activity, including clinical isolates of methicillin-resistant *Staphylococcus aureus* (*MRSA*), as well as reference strains *Escherichia coli* (*E.coli*) ATCC 25922 from Al Salam Hospital, Cairo, Egypt. Fresh bacterial cultures were grown to a concentration of 104 CFU mL$^{-1}$ (0.5 McFarland) in Luria–Bertani (LB) broth by incubating at 37 °C for 24 hours. For the antibacterial assays, 50 μL of each culture was gently spread on LB agar plates to create bacterial lawns. Four 8 mm wells were then punched in the agar using a cork borer for testing the antibacterial agents.

**2.6.1. Antibacterial potentials of CaO, ZnFe-LDH and CaO/ZnFe-LDH.** The antibacterial activity of CaO, ZnFe-LDH and CaO/ZnFe-LDH against *MRSA* and *E.coli* was evaluated using the agar well diffusion assay. Briefly, 100 μL of CaO, 10 mg per mL ZnFe-LDH, 1 mg per mL CaO/ZnFe-LDH, DMSO (negative control), or 1.5 mg per mL ampicillin (positive control) were added into the wells punched in agar plates pre-seeded with the bacterial cultures. After incubating the plates for 24 hours at 37 °C, the diameters of the zones of inhibition surrounding each well were measured in mm using a ruler.

**2.6.2. Minimal inhibitory concentration (MIC) measurement.** The antibacterial activity was measured using the minimum inhibitory concentration (MIC) technique. To create serial two-fold dilutions, stock solutions of the test chemicals were made in DMSO and then further diluted in Mueller–Hinton broth for bacteria. For the bacterial and fungal strains under test, final cell concentrations of roughly 106 CFU mL$^{-1}$ were attained by adding these dilutions to each well of a 96-well microtiter plate. After being sealed, the plates were incubated for 24 hours at 37 °C. The lowest concentration of test agent that prevented turbidity from being visible during incubation was determined to be the MIC values. For reproducibility, each experiment was run in triplicate.

### 2.7. Greenness profile determination

Numerous factors influence the environmental friendliness of an analytical methodology, including the quantity and toxicity of chemicals used, waste production, power consumption, process complexity, miniaturization, and automation. To assess the greenness of a method, two green measures were employed: the Analytical Eco-scale and the Analytical GREEnness Calculator (AGREE). The first method, the Eco-scale score, is calculated by subtracting the total number of penalty points, based on waste, toxicity, reagents, and power, from one hundred. This score allows researchers to gauge the method's environmental efficiency. AGREE, another metric, is a quantitative tool that generates a score reflecting how well a method adheres to the twelve main principles of green analytical chemistry.

## 3 Results and discussion

### 3.1. Characterization of prepared materials

X-ray diffraction patterns of synthesized materials are presented in Fig. 2(a)–(c). The XRD pattern of ZnFe-LDH seemed to be highly crystalline structure (Fig. 2(a)), as evidenced with much sharper diffraction peaks. The typical diffraction peaks of ZnFe-LDH were observed at the $2\theta$ values = 9.3°, 18.4°, 33.1°, and 58.3° corresponding respectively to crystals (003), (006), (009) and (110) planes.[20–24] In (Fig. 2(b)) the CaO exhibited prominent peaks at $2\theta$ values of 34.3°, 47.41°, 51.17°, and 62.62°, corresponding to the (111), (200), (220), and (311) planes of CaO,[25] respectively. The presence of Ca(OH)$_2$ is also observed in (Fig. 2(b)) as indicated by diffraction peaks at 18.0 °and 28.9°. Because of the oxygen anion that is produced on its surface, calcium oxide has high basic properties. When this compound is exposed to ambient air, $H_2O$ from the air reacts with its strong basic surface to form Ca(OH)$_2$.[26] The peaks of all composites were mainly superimposed on CaO and ZnFe-LDH, and the main peaks of were observed. By comparing the XRD diffraction spectra, it can be found that for the composite materials, CaO and ZnFe-LDH recombination occurred. From (Fig. 2(c)), in the composite chart, the peak at (003) became narrow and of low intense, the peaks at (006) decreased, the peak at (009) became more sharp and increase in intense, the peak at (111) became of
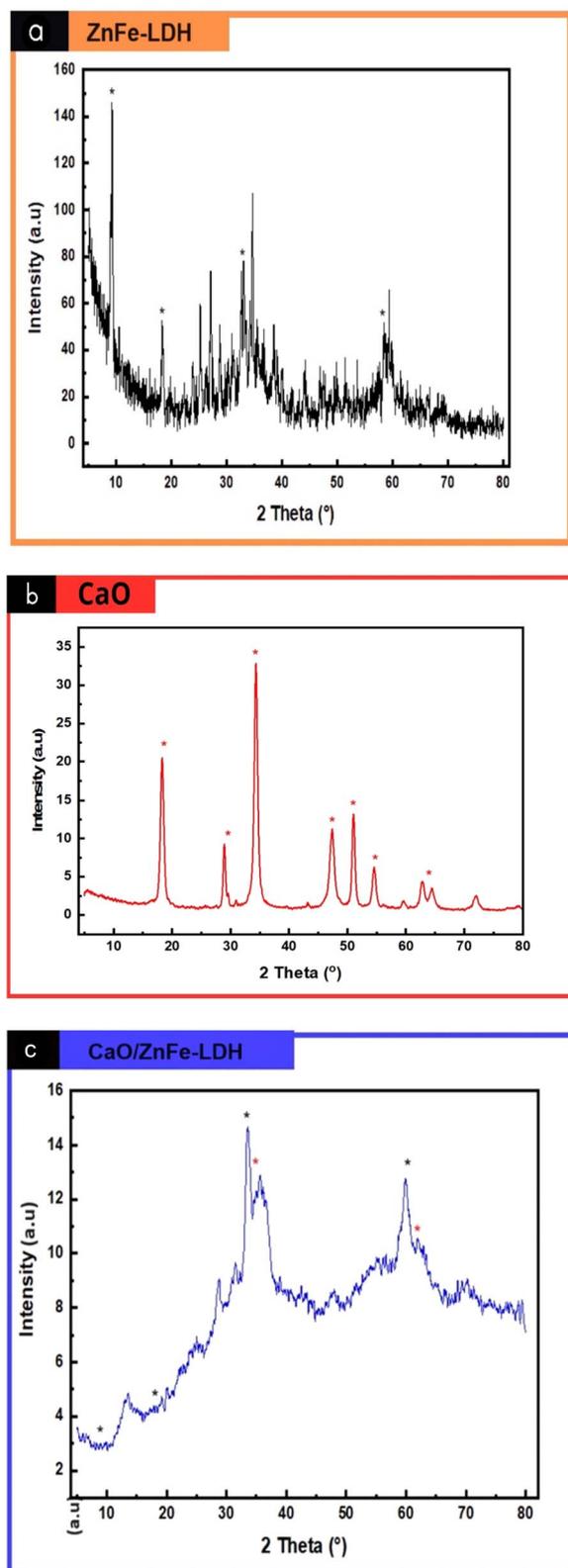
Fig. 2  The XRD pattern of the synthesized (a) ZnFe-LDH, (b) CaO and (c) CaO/ZnFe-LDH.

low intense, the intensity of the peak at 59.93° (110) increased and became broader, and the intensity of the peak at (311) decreased, indicating interaction between LDH and CaO. These

changes suggest the successful formation of the CaO/ZnFe-LDH nanocomposite.

As observed in Fig. 2(c) that there are shifts of this (003) and (006) peaks are attributed to the replacement of $Zn^{2+}$ by other $Ca^{2+}$ metal ions.[27–29] The replacement of the $Zn^{2+}$ (ionic radius = 74 Å) by the larger $Ca^{2+}$ (ionic radius ~ 1.00 Å) results the increase of interlayer distance space from 1.29014 Å nm of LDH to 1.394527 Å of the composite one. Also, the iterance of $Ca^{2+}$ ion in the LDH lattice showed a deviation in main peaks, with reduced intensities and broadening of the peaks, which confirms the successfully prepared composite samples.[30] The formation of LDH phases in the present of calcined eggshell and trivalent metal and divalent metal ions solution can be explained as follows.[31]

$Ca(OH)_2$ is formed by the reaction of calcined eggshells and water. $Ca^{2+}$, $NO_3^-$, and $OH^-$ were deposited on the surface of LDH particles to form doped LDHs with Ca metal ions. The process that LDH starts from nucleation to growth can be given by the following reactions (4) and (5):

$$CaCO_3 \rightarrow CaO + CO_2, 900\ °C \tag{4}$$

$$CaO + H_2O \rightarrow Ca(OH)_2 \rightarrow Ca^{2+} + 2OH^- \tag{5}$$
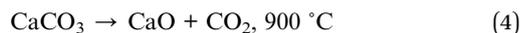
Crystallite calculated using the Scherrer equation the Scherrer equation $CZ = (0.94\lambda)/(\beta \cos\theta)$, where $\theta$ is the incident X-ray wavelength (Cu-K$\alpha$ = 0.154 nm), $\beta$ is the full width at half maximum, and $\theta$ is the Bragg's angle Scherrer equation ($D = K\lambda/\beta \cos\theta$).[32] The crystal sizes were 10.79 nm for ZnFe-LDH, 2.15 nm for CaO/ZnFe-LDH, and 8.53 nm for CaO. The changes in crystallite size values confirm the formation of the composite material.

Fig. 3 illustrates that the FTIR spectrum of the synthesized ZnFe-LDH displays multiple peaks consistent with those reported in previous studies. The broad band at 3401 $cm^{-1}$ is associated with the stretching vibration of hydroxyl groups in the LDH, as well as interlayer and adsorbed water molecules. The band at 1630 $cm^{-1}$ corresponds to the bending vibration of water ($\nu$H–O–H). The strong band at 1391 $cm^{-1}$ matches the vibration mode of nitrate ions ($NO_3^-$). Bands below 1000 $cm^{-1}$ are likely related to the stretching vibrations of M–O and M–O–M bonds in the LDH.[22,24,33] The carbonate group's out-of-plane vibration modes are attributed to the spectrum peak at 872 $cm^{-1}$ in the CaO support, while the C–O stretching vibrations are observed as a strong peak at 1053 $cm^{-1}$ and a weak peak at 1093 $cm^{-1}$. The asymmetric stretching of the C=O group in $CO_3^{2-}$ anions is clearly seen near 1455 $cm^{-1}$. The prominent peak at 3640 $cm^{-1}$ corresponds to the OH group in $Ca(OH)_2$, which formed when CaO adsorbed water. Additionally, a broader band around 3425 $cm^{-1}$ is associated with the bending mode of OH groups from physically adsorbed moisture on the surface.[25,34]

In the CaO/ZnFe-LDH spectrum, the absorbance band at 3413 $cm^{-1}$ shows a noticeable increase in intensity, likely due to O–H stretching of absorbed water. Peaks around 1517 $cm^{-1}$ and 1391 $cm^{-1}$ were displaced, with the former attributed to the C=C stretching band and the latter to the $NO_3^-$ group
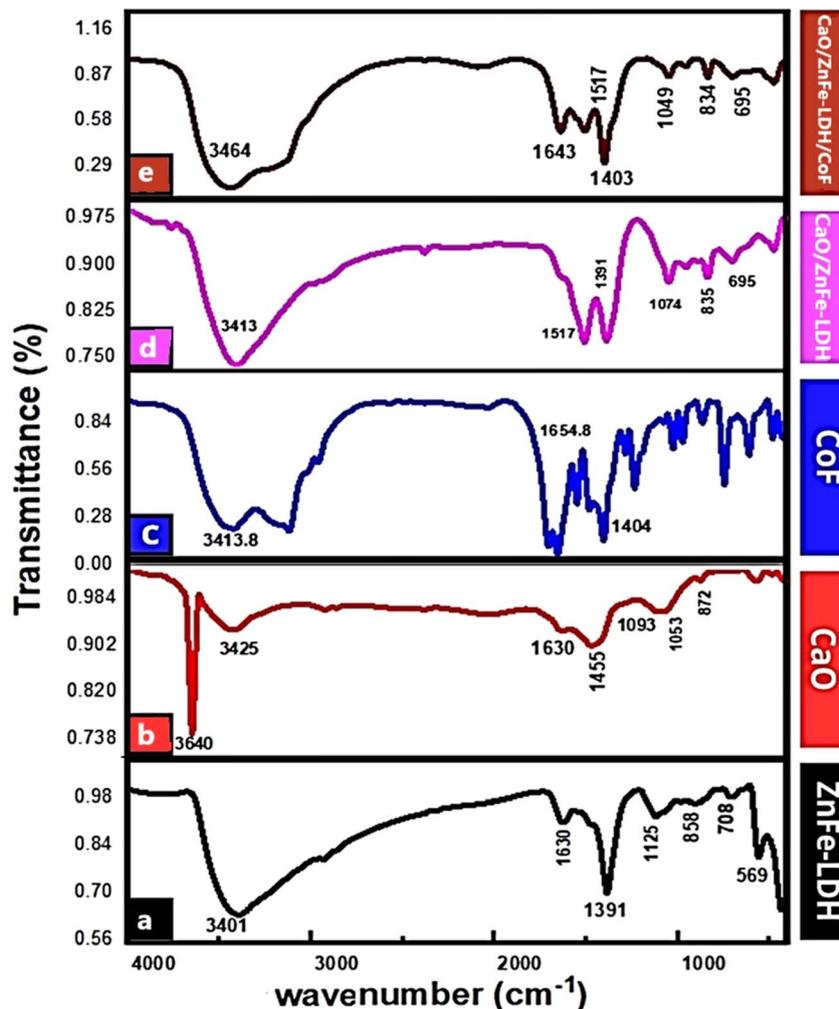
Fig. 3  FTIR analysis of the synthesized ZnFe-LDH, CaO, COF, CaO/ZnFe-LDH and CaO/ZnFe-LDH/COF.

stretching vibration, resulting in a reduced intensity at $1391 \text{ cm}^{-1}$. Additional bands below $1000 \text{ cm}^{-1}$ were identified as M–O vibration modes of layered double hydroxide complexes. The O–M–O vibration in the brucite-like LDH layers was observed between 400 and $500 \text{ cm}^{-1}$, and a peak at $835 \text{ cm}^{-1}$ indicated the M–O vibration mode, confirming the interaction between LDH and CaO.

To obtain detailed information about the specific surface area and porosity of the catalyst, a nitrogen adsorption measurement was conducted. Fig. 4 shows the $N_2$ adsorption–desorption isotherms and the corresponding pore-size distribution curves for CaO, ZnFe-LDH, and CaO/ZnFe-LDH. The isotherm for ZnFe-LDH is classified as a type IV isotherm with a type H3 hysteresis loop according to IUPAC standards, confirming the mesoporous nature of these samples. When ZnFe-LDH is combined with CaO, its physicochemical characteristics, as detailed in Table 2, decrease. This change is likely due to a shift in the microstructure caused by the presence of different cations within the structure.[21,23,24] The CaO is classified as a type III isotherm and exhibits an H4 hysteresis loop. It has the largest pore size among the three materials and the lowest
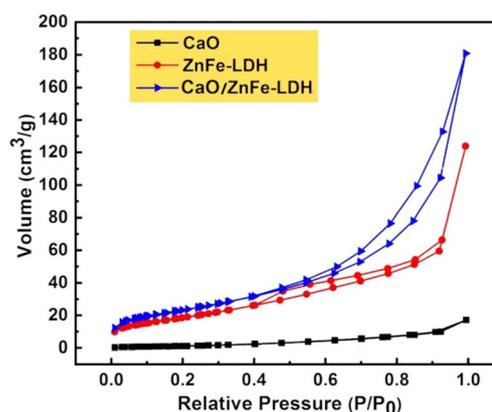


Fig. 4  Nitrogen adsorption–desorption isotherms curves for the prepared adsorbents.

surface area, which indicates an irregular shape and a broad size distribution.[35] The synthesized CaO/ZnFe-LDH nanocomposite exhibits a type III isotherm with an H3 hysteresis loop, indicating the presence of aggregates of plate-like

**Table 2** The physico-chemical properties of the materials catalyst

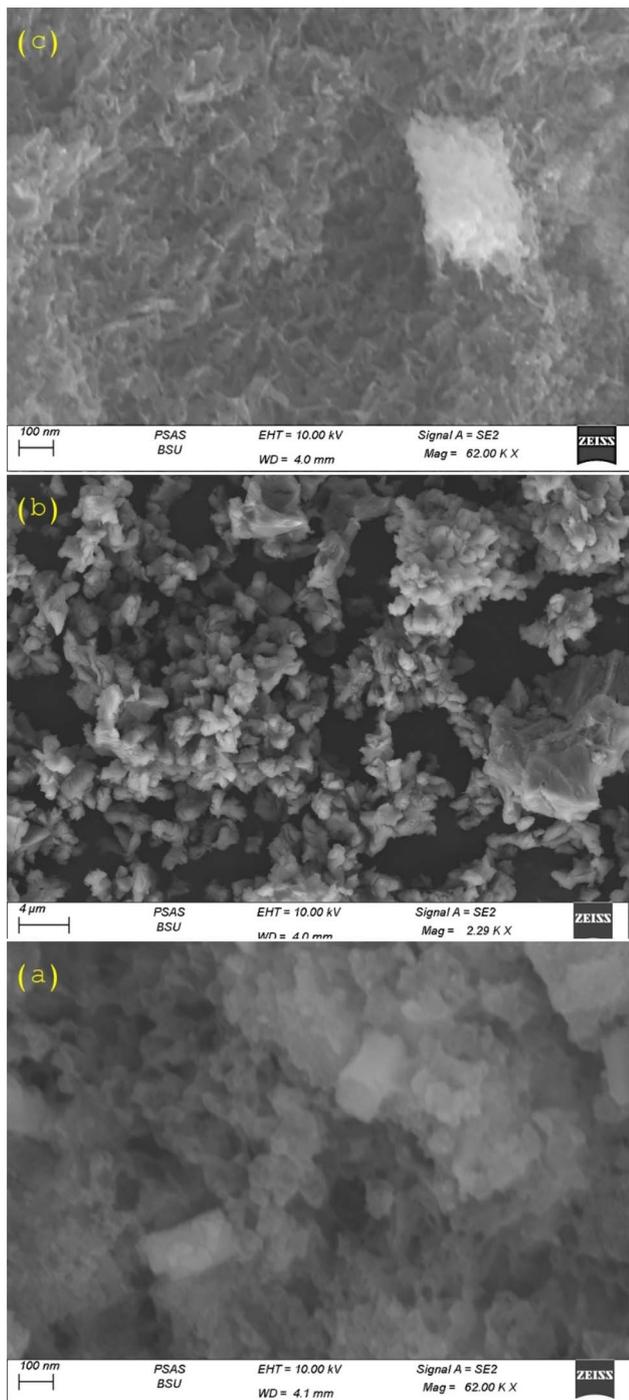| Catalyst | Pore size (nm) | Pore volume (cm$^3$ g$^{-1}$) | Surface area (m$^2$ g$^{-1}$) |
|---|---|---|---|
| CaO | 18.38 | 0.03 | 5.62 |
| ZnFe-LDH | 10.89 | 0.19 | 69.23 |
| CaO/ZnFe-LDH | 12.98 | 0.28 | 84.78 |

**Fig. 5** SEM images for the ZnFe-LDH (a), CaO (b), and CaO/ZnFe-LDH (c).

particles that constitute mesoporous materials, as demonstrated by the SEM images in Fig. 5. It also shows the highest surface area, pore volume, and pore size, as detailed in Table 2, reflecting the material's high absorptivity characteristics. The pore size range of 2–50 nm confirms its classification as a mesoporous material. The pore size distribution curves for the prepared adsorbents are presented in Fig. 6.

SEM images for CaO, ZnFe-LDH and CaO/ZnFe-LDH are presented in Fig. 5(a)–(c). The ZnFe-LDH, produced by co-precipitation, exhibits stacked plates with a clear layered structure. It shows specific aggregation between layers and a distinct lamellar structure, along with a disordered state. Additionally, it reveals a distinctive hexagonal-like morphology, high porosity, and layered sheets typical of LDH materials[9,21–24,33] Fig. 5(a). The CaO structure in Fig. 5(b) resembles a beehive and exhibits an agglomerated particle catalyst texture, with a morphology akin to clusters of grapes. This demonstrates a heterogeneous distribution of structural clusters, often composed of irregularly shaped particles. The irregular micro-morphology and the range of sizes and shapes may contribute to its greater catalytic activity.[36–40] The CaO/ZnFe-LDH shown in Fig. 5(c) displays increased porosity in the composite material and a fibrous, agglomerated structure. Following preparation, the composite layer facilitates the incorporation of CaO. EDX analysis confirmed the presence of Zn, Fe, O, and Ca in the prepared materials (Fig. 1(a)–(c)).

To study the thermal stability of the fabricated adsorbents, the thermal behavior of ZnFe-LDH, CaO, and CaO/ZnFe-LDH was investigated using TGA/DTG. As shown in Fig. 7, the TGA thermogram reveals two main weight loss events, characteristic of LDH materials, at distinct temperature ranges. The first weight loss, occurring between 50 and 200 °C, is associated with the loss of surface water molecules that have been physisorbed. The second weight loss, occurring in the temperature range of 250–500 °C, is linked to the decarboxylation of nitrate anions, which leads to the collapse of the layered structure and the removal of interlayer anions.[41,42] The approximately 8.80% weight loss in CaO, observed between 50 and 450 °C, is attributed to the evaporation of free moisture and the decomposition of calcium hydroxide (Ca(OH)$_2$) to produce CaO and H$_2$O.[25] The weight loss continued to decrease until 800 °C. The thermal stability of CaO/ZnFe-LDH was higher than that of ZnFe-LDH. Therefore, the addition of CaO to ZnFe-LDH enhanced the thermal stability of CaO/ZnFe-LDH (Fig. 7(a)–(c)).

### 3.2. COF uptake investigation

Pollutant removal from wastewater is greatly influenced by pH, which alters the ionization states of COF molecules and leads to the creation of distinct binding sites, while also affecting the adsorbent's surface charge. The impact of pH (ranging from 3 to 9) on COF adsorption onto ZnFe-LDH and CaO/ZnFe-LDH nanomaterial samples is shown in Fig. 8(a) (with an initial concentration of 20 mg per L COF, an adsorbent dosage of 0.01 g, and a temperature of 25 ± 1 °C). The results demonstrate that the pH of the solution significantly impacts the effectiveness of the materials for COF removal, with ZnFe-LDH showing
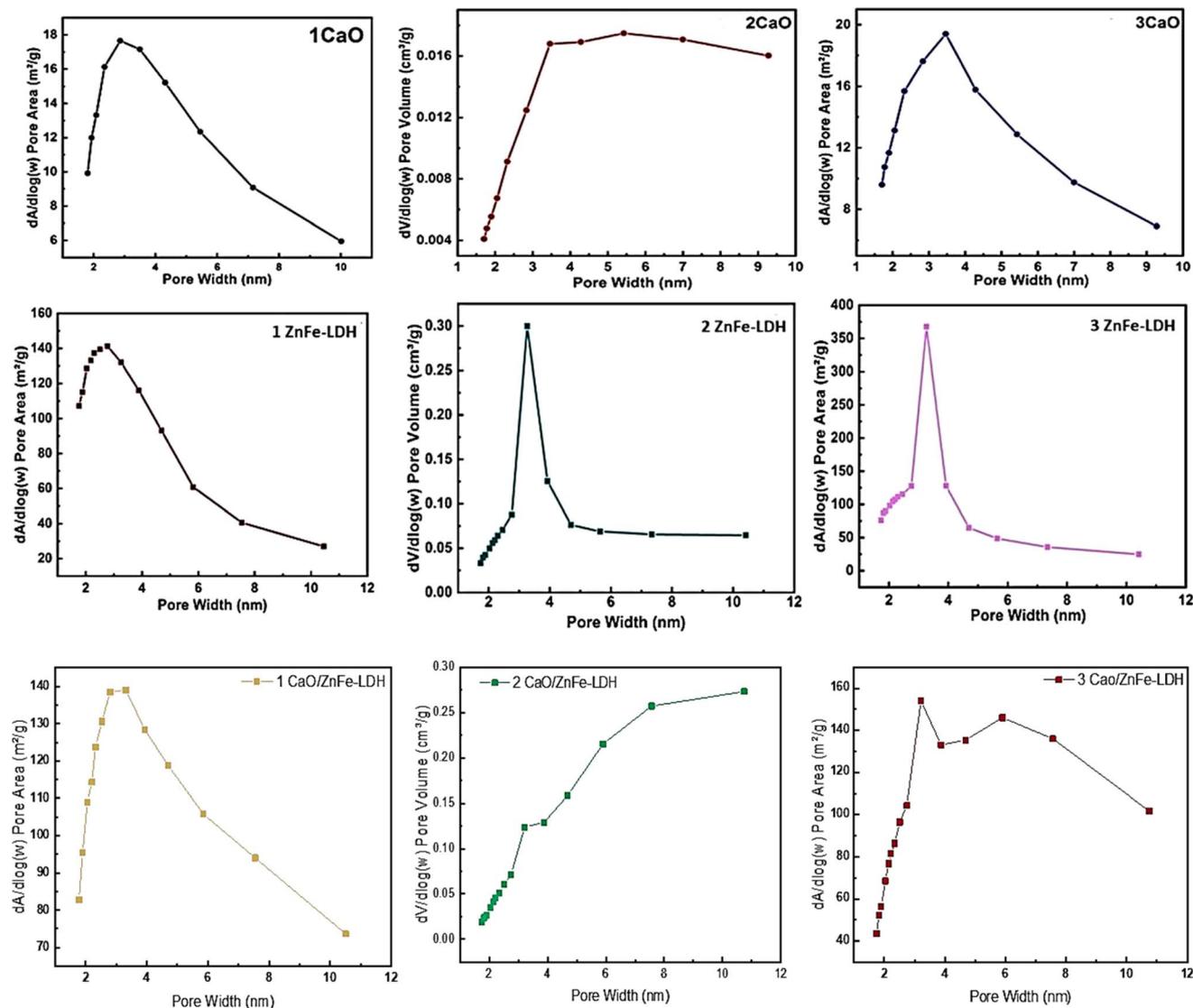
**Fig. 6** The pore size distribution curves for the prepared adsorbents.

maximum effectiveness at pH 9 and CaO/ZnFe-LDH at pH 7. At pH 9, the surface charge of ZnFe-LDH may be more favorable for attracting and binding COF molecules, thus facilitating the adsorption process. Conversely, COF is more soluble at lower pH values, so maintaining a pH of 7 helps control COF solubility, preventing it from staying in solution and allowing better adsorption onto CaO/ZnFe-LDH. The PZC values recorded were ZnFe-LDH = 7.6 and CaO/ZnFe-LDH = 8.2, as shown in Fig. 8(b). COF has a $pK_a$ of 10.4, meaning that at pH values below 10.4, the molecule is fully protonated.[43] The choice of pH 7 for the adsorption of COF using CaO/ZnFe-LDH is related to the $pK_a$ (acid dissociation constant) of COF, which represents the pH at which the compound is half-dissociated into its ionized and non-ionized forms. For ZnFe-LDH, pH 9 is chosen to maximize interaction with the ionized form of COF, as the COF molecules are predominantly ionized at this pH, enhancing their affinity for the adsorbent surface. Conversely, at pH 7, COF molecules are less likely to be ionized, which can

increase their affinity for the CaO/ZnFe-LDH adsorbent. Additionally, pH 7 may be selected to ensure the stability and activity of the CaO/ZnFe-LDH adsorbent during the adsorption process, as some adsorbents perform optimally within a specific pH range. Overall, pH 7 is likely chosen to maintain COF in its non-ionized form, promoting favorable interactions with the CaO/ZnFe-LDH adsorbent and ensuring the stability of the adsorbent throughout the process.

Using ZnFe-LDH and CaO/ZnFe-LDH in amounts ranging from 0.01 to 0.1 g per 20 mL COF solution at pH 7 and a starting concentration of 25 ppm for 24 hours, the COF elimination efficiency is demonstrated in Fig. 8(c). The data show that the COF removal rate increases with the adsorbent dosage, reaching a maximum at 0.05 g. Consequently, as the adsorbent dose increases, the number of active sites available for adsorption also increases.[44]

Adsorption isotherm studies reveal the distribution of molecules between the solid and liquid phases at equilibrium
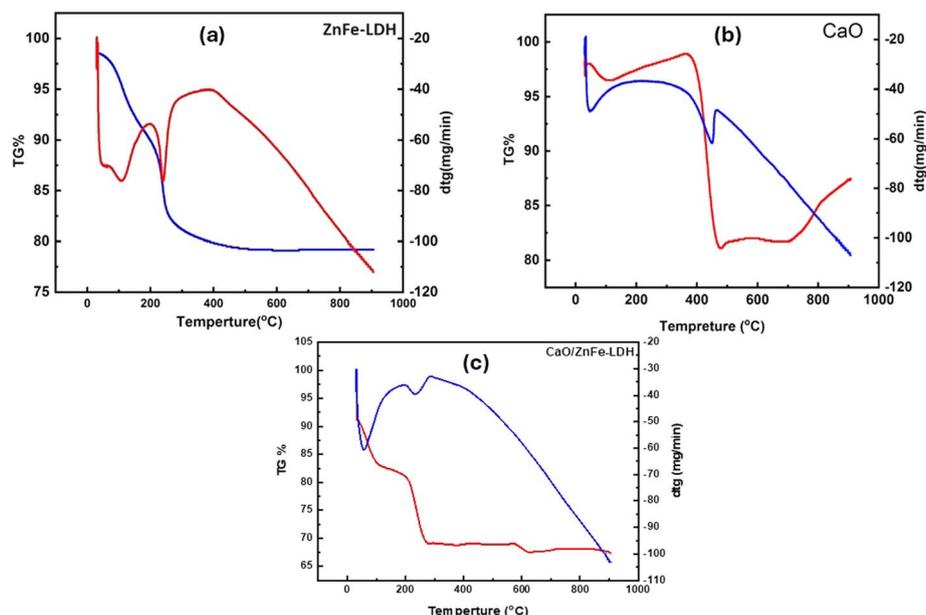
Fig. 7 TGA/DTG thermograms of (a) ZnFe-LDH, (b) CaO and (c) Cao/ZnFe-LDH.

during the adsorption process.[45] Adsorption isotherm studies provide crucial insights into the mechanisms by which an adsorbent removes an adsorbate. COF concentrations ranging from 10 to 1000 mg $L^{-1}$ were investigated in relation to the equilibrium adsorption of COF onto ZnFe-LDH and CaO/ZnFe-LDH. The non-linear fitting method was used to analyze COF adsorption on the surfaces of ZnFe-LDH and CaO/ZnFe-LDH. Equilibrium data were evaluated using Langmuir, Freundlich, Sips, Baudu, Langmuir–Freundlich, and Fritz–Schlunder isotherm models. The correlation coefficient values for the adsorption isotherm constants are summarized in Table 3, and their plots are shown in Fig. 9. For COF sorption, the Langmuir model yielded $R^2$ values of 0.9922 for ZnFe-LDH and 0.9977 for CaO/ZnFe-LDH. The Freundlich isotherm provided lower $R^2$ values of 0.964 for ZnFe-LDH and 0.98 for CaO/ZnFe-LDH. This indicates that the Langmuir isotherm fits the data better for both ZnFe-LDH and CaO/ZnFe-LDH, accurately representing the sorption characteristics of COF. According to the Langmuir isotherm calculations, the highest COF adsorption capacities were 152.35 mg $g^{-1}$ for ZnFe-LDH and 194.87 mg $g^{-1}$ for CaO/ZnFe-LDH, suggesting that COF is uniformly distributed in a monolayer on the adsorbent surfaces, reaching a dynamic equilibrium state.

### 3.3. Adsorption kinetics

The study of adsorption kinetics is crucial for understanding the effectiveness of adsorbents, as it provides essential information about the processes and the rate at which pollutants are adsorbed. Adsorption kinetics involves four key processes: bulk diffusion, film diffusion, intra-particle diffusion, and adsorption onto the adsorbent's surface.[46] Table 4 presents the relevant constants and variables, along with the nonlinear relationships of the kinetics models for COF adsorption using

ZnFe-LDH and CaO/ZnFe-LDH. The equilibrium COF adsorption increased over time, reaching a plateau between 0 and 250 minutes. Initially, the adsorption rate was rapid; it then stabilized after 50 minutes for ZnFe-LDH and 20 minutes for CaO/ZnFe-LDH. This rapid adsorption can be attributed to the swift diffusion of drug residues onto the adsorbent's surface in aqueous environments.[47] The significant presence of active sites on the adsorbent may have contributed to the initial increase in sorption efficiency.[48] The value of $R^2$ and $q_{e,cal}$ for COF adsorption is higher for the 1,2-mixed order and Avrami kinetic models compared to other kinetic models, as shown in Table 4. The corresponding $R^2$ values are detailed in Table 4. Fig. 10(a) and (b) demonstrate that COF adsorption by ZnFe-LDH is more accurately described by the 1,2-mixed order and Avrami kinetic models ($R^2 = 0.98$) than by the first order and second order kinetic models ($R^2 = 0.97$ and $R^2 = 0.9622$, respectively). The mixed order kinetic model indicates that adsorption occurs through both electron sharing or covalent interactions and physical bond formation, such as hydrogen bonds, suggesting that the reaction kinetics are governed by both chemical and physical adsorption. Additionally, the composite material exhibits different adsorption modes towards COF due to physical adsorption, as it fits well with the pseudo-first order model. As adsorption time progresses, the adsorption sites on the adsorbent become occupied by COF, leading to a decrease in the adsorption rate.

### 3.4. Real water samples analysis

The removal of COF using 5 ppm concentration, pH 7, and 0.05 g of CaO/ZnFe-LDH was evaluated with real water sources, including tap water, River Nile water, and wastewater samples. The corresponding removal efficiencies of the nanocomposites
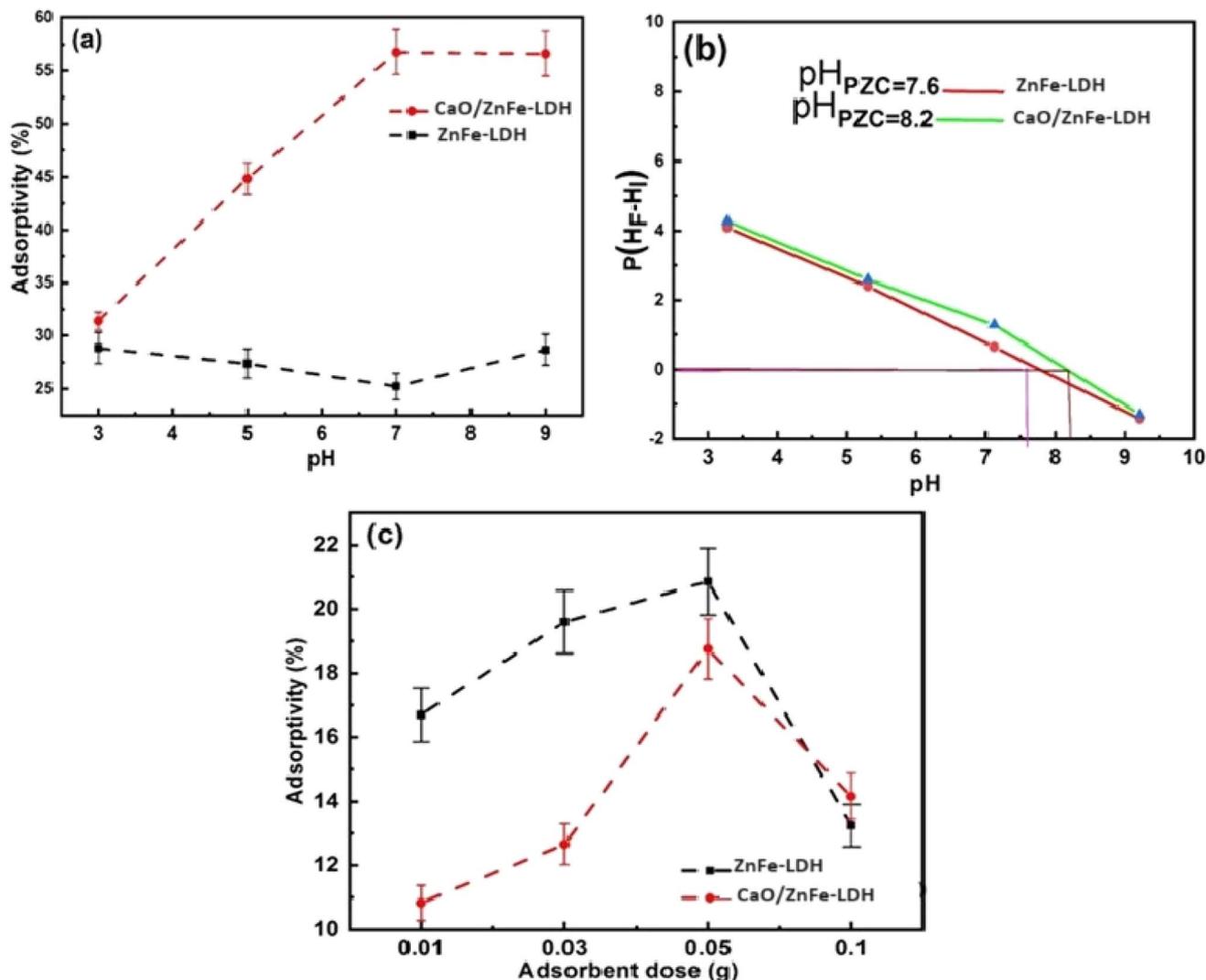
Fig. 8 Effect of (a) pH, (b) pH$_{pzc}$ and (c) amount of adsorbents (g) on the removal percent of COF with an initial concentration of 20 mg per L COF, an adsorbent dosage of 0.01 g, and a temperature of 25 ± 1 °C.

were 17.22% for tap water, 10.38% for River Nile water, and 30.41% for wastewater.

### 3.5. Desorption study

To assess the applicability of a particular adsorbent, desorption and regeneration procedures must be conducted. Ineffective desorption or regeneration can lead to decreased adsorbent efficacy and potential secondary environmental degradation. As shown in Fig. 11(a), the desorption efficiencies achieved were 95.81% with DMF, 91.83% with methanol, and 94.82% with isopropanol after 48 hours.

### 3.6. Recyclability of the nano-adsorbent

One of the most critical factors in evaluating the economic viability of used adsorbents is their reusability. As shown in Fig. 11(b), after four cycles, there was no significant change in the adsorption capacity of CaO/ZnFe-LDH, indicating that the

decrease in active sites was minimal. This suggests that the material exhibits excellent recovery behavior.

### 3.7. Mechanism of the adsorption

CaO/ZnFe-LDH showed promising maximum adsorption capacity for COF. As shown in Table 3, CaO/ZnFe-LDH shows very promising values of maximum adsorption capacity for COF to other similar materials in the literature (Table 1). Even for materials that show higher performance, the cost of CaO/ZnFe-LDH is competitive compared to that of such materials. For such promising adsorbents, insights into the adsorption mechanism are necessary to aid in further development of their performance for real-life adsorption applications. The results from the FTIR spectra after adsorption can be very useful for obtaining insights into the possible interactions between COF with CaO/ZnFe-LDH. The FTIR characteristic bands after the adsorption of COF on composite material are also shown in Fig. 3. CaO/ZnFe-LDH/COF showed the same characteristic

**Table 3** Summarizes the model equations and correlation coefficient values for the adsorption isotherm constant

| Model | Parameter | ZnFe-LDH | CaO/ZnFe-LDH |
|---|---|---|---|
| Langmuir $q_e = q_{max} \dfrac{K_L\, C_e}{1 + K_L C_e}$ | $q_{max}$ | 152.35 | 194.87 |
| | $K_L$ | 0.06 | 0.05 |
| | $R^2$ | 0.99 | 0.99 |
| Freundlich $q_e = K_F C_e^{1/n}$ | $1/n$ | 0.55 | 0.64 |
| | $K_F$ | 14.84 | 13.85 |
| | $R^2$ | 0.96 | 0.98 |
| Sips $q_e = \dfrac{q_{max} K_s (C_e)^{1/ns}}{1 + K_s (C_e)^{1/ns}}$ | $q_{max}$ | 123.72 | 154.41 |
| | $K_s$ | 0.05 | 0.04 |
| | $1/n$ | 1.35 | 1.24 |
| | $R^2$ | 0.99 | 0.99 |
| Langmuir $-$ Freundlich $q_e = \dfrac{q_{max} (K_{LF} C_e)^{MLF}}{1 + (K_{LF} C_e)^{MLF}}$ | $q_{MLF}$ | 123.72 | 154.40 |
| | $K_{LF}$ | 0.10 | 0.08 |
| | $M_{LF}$ | 1.35 | 1.24 |
| | $R^2$ | 0.99 | 0.99 |
| Baudu $q_e = \dfrac{q_{max}\, b_o\, C_e^{1+x+y}}{1 + b_o C_e^{1+x}}$ | $q_m$ | 123.7192 | 154.3979 |
| | $b_o$ | 0.05 | 0.04 |
| | $X$ | 0 | 0 |
| | $Y$ | 0.35 | 0.24 |
| | $R^2$ | 0.99 | 0.99 |
| Fritz $-$ Schlunder $q_e = \dfrac{q_{max} K_1 C_e^{m_1}}{1 + K_2 C_e^{m_2}}$ | $q_{mFSS}$ | 33.99 | 29.63 |
| | $K_1$ | 0.54 | 0.47 |
| | $K_2$ | 0.23 | 0.01 |
| | $m_1$ | 0.55 | 0.64 |
| | $m_2$ | $0.30 \times 10^{-4}$ | 0 |
| | $R^2$ | 0.96 | 0.98 |
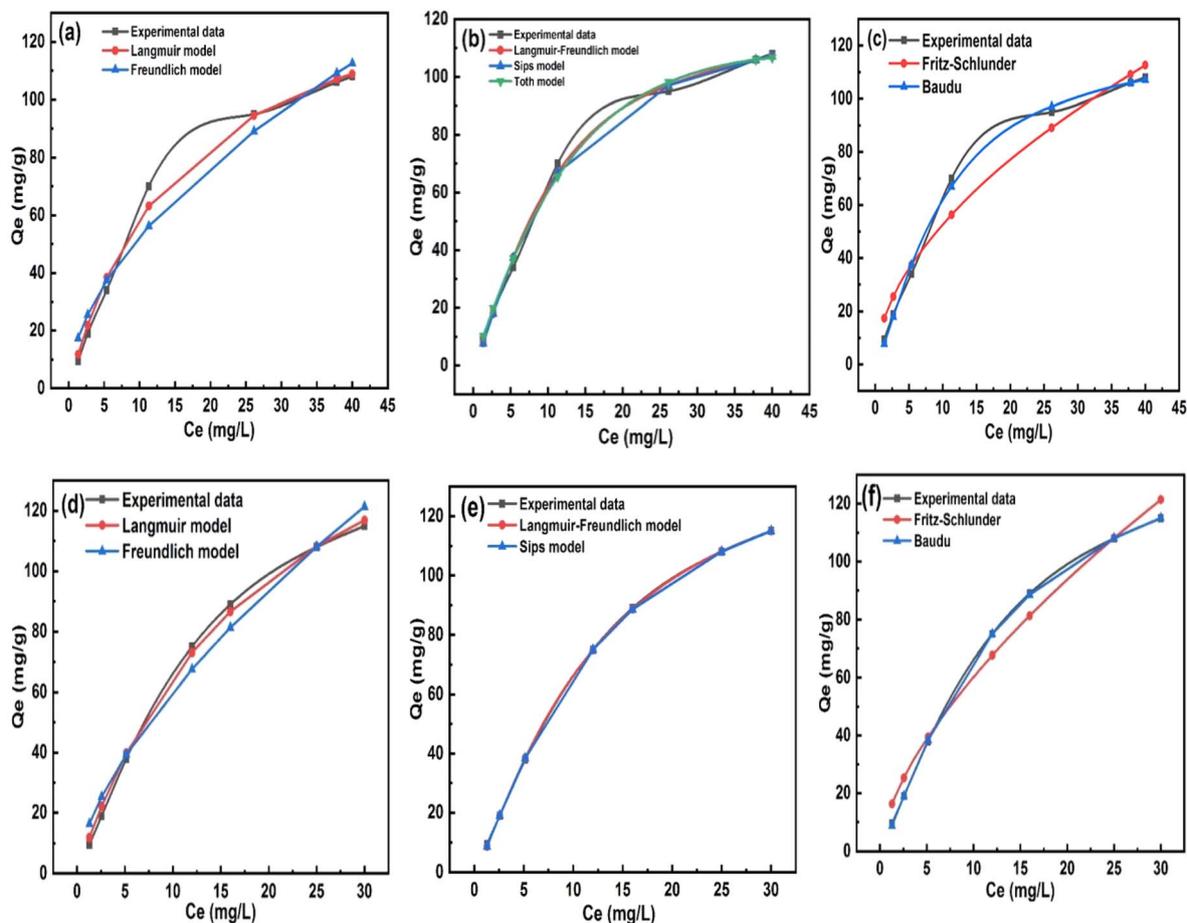


**Fig. 9** Best fit isotherm model for COF adsorption onto (a–c) ZnFe-LDH and (d–f) CaO/ZnFe-LDH.

**Table 4** A summary of nonlinear kinetic models for COF on ZnFe-LDH and CaO/ZnFe-LDH

| Kinetic models | Equation | Parameters | ZnFe-LDH | CaO/ZnFe-LDH |
|---|---|---|---|---|
| Pseudo first order | $q_t = q_e(1 - e^{-K_1 t})$ | $K_1$ | 0.08 | 0.14 |
| | | $Q_e$ | 5.14 | 6.25 |
| | | $R^2$ | 0.97 | 0.98 |
| Pseudo second order | $q_t = \dfrac{q_e^2 K_2 t}{1 + q_e K_2 t}$ | $K_2$ | 0.02 | 0.03 |
| | | $Q_e$ | 5.62 | 6.76 |
| | | $R^2$ | 0.96 | 0.96 |
| Mixed 1,2 order | $q_t = q_e \dfrac{1 - e^{-Kt}}{1 - f_2 e^{-Kt}}$ | $K$ | 0.08 | $9.99 \times 10^{-5}$ |
| | | $Q_e$ | 5.14 | 6.77 |
| | | $F_2$ | 0.00 | 0.99 |
| | | $R^2$ | 0.98 | 0.96 |
| Avrami | $q_t = q_e(1 - [e^{-K_{av}t}]^{n_{av}})$ | $Q_e$ | 5.14 | 6.25 |
| | | $K_{av}$ | 0.29 | 2.07 |
| | | $n_{av}$ | 0.28 | 0.07 |
| | | $R^2$ | 0.98 | 0.98 |
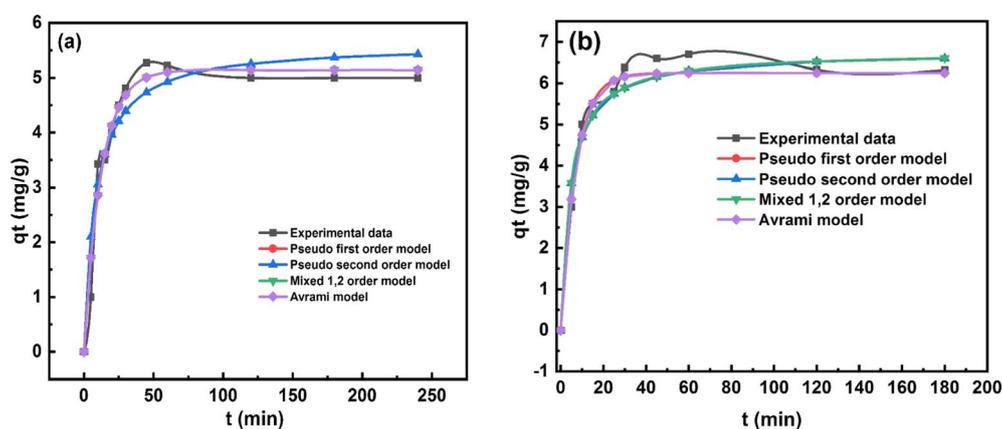


Fig. 10 Kinetic models fitting for the COF adsorption onto (a) ZnFe-LDH and (b) CaO/ZnFe-LDH.
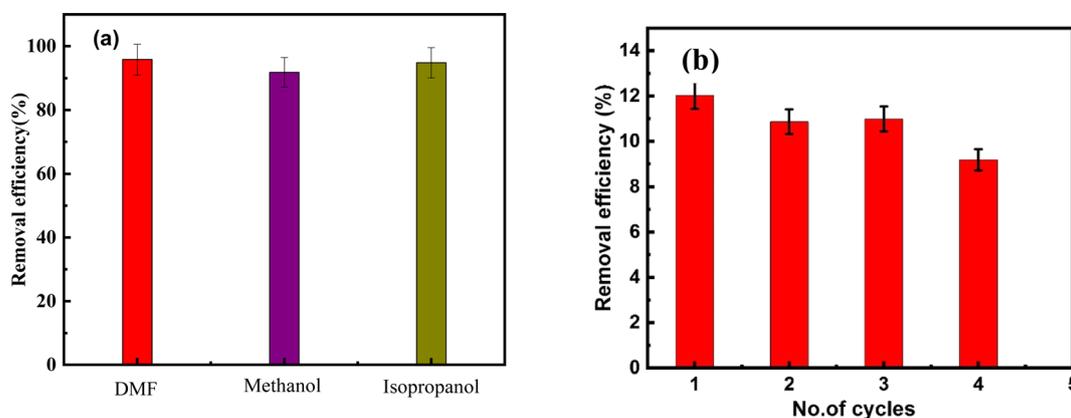


Fig. 11 Desorption of COF using different eluents (a) and the reusability performance of CaO/ZnFe-LDH (b).

bands as CaO/ZnFe-LDH, with some changes. The 3413 cm⁻¹ band shifted to 3464 cm⁻¹ for CaO/ZnFe-LDH/COF, and become more a broader pattern. The C–O peak at 1403, 834, and 695 cm⁻¹ was more intense and broader than that of CaO/ZnFe-LDH, suggesting the existence of an adsorption interaction due to the between COF and composite material. As shown in Fig. 3,

possible hydrogen bonding between hydrogen atoms in COF and oxygen in CaO, ZnFe-LDH in composite material CaO/ZnFe-LDH could represent one of the main mechanisms for COF adsorption over CaO/ZnFe-LDH. The mechanism of the interaction between COF and the composite material was shown in Scheme 2.
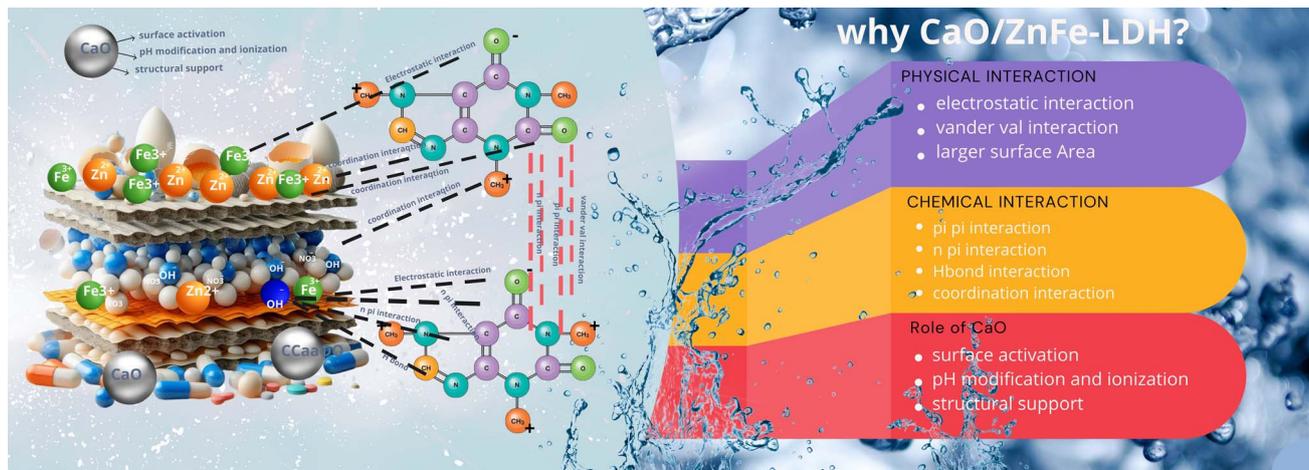
**Scheme 2** The mechanism of the material and COF.
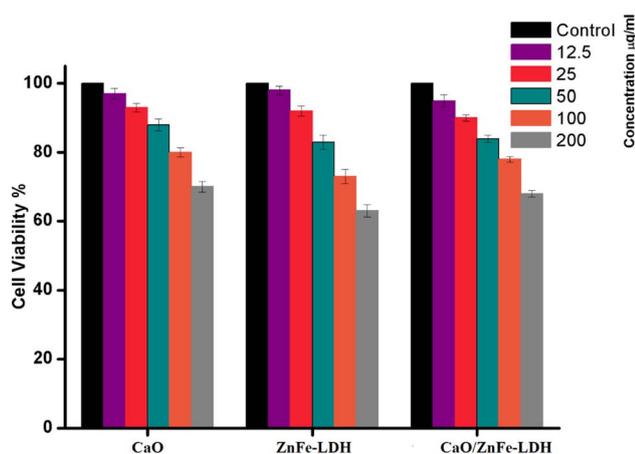


**Fig. 12** Cell viability (%) after incubation 48 h with CaO, ZnFe-LDH, and CaO/ZnFe-LDH, ($n = 3$) $\pm$ SD.
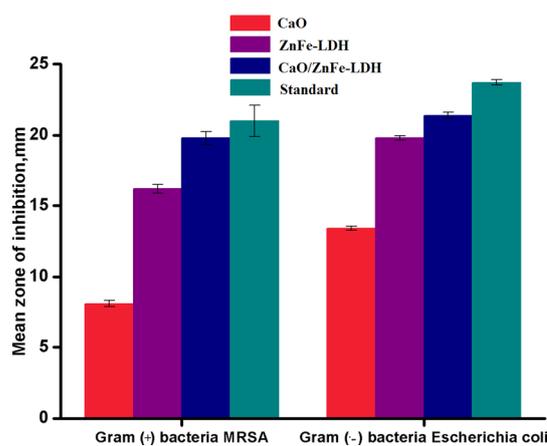


**Fig. 13** The mean $\pm$ SD of triplicates was used to determine the antibacterial activity of CaO, ZnFe-LDH, and CaO/ZnFe-LDH against standard antibiotics of *E.coli* and *MRSA*. The zone of inhibition diameters in mm were measured.

**Table 5** The antimicrobial efficacy of CaO, ZnFe-LDH, and CaO/ZnFe-LDH and the average zone of inhibition in mm, $\pm$ standard deviation beyond well diameter (6 mm)

| Compounds | Gram (+) bacteria *MRSA* | Gram (-) bacteria *Escherichia coli* |
|---|---|---|
| Standard | 21.5 $\pm$ 1.1 mm | 23.7 $\pm$ 0.19 mm |
| ZnFe-LDH | 16.2 $\pm$ 0.31 mm | 19.8 $\pm$ 0.16 mm |
| CaO NPs | 8.1 $\pm$ 0.21 mm | 13.4 $\pm$ 0.15 mm |
| CaO/ZnFe-LDH | 19.8 $\pm$ 0.45 mm | 21.4 $\pm$ 0.21 mm |

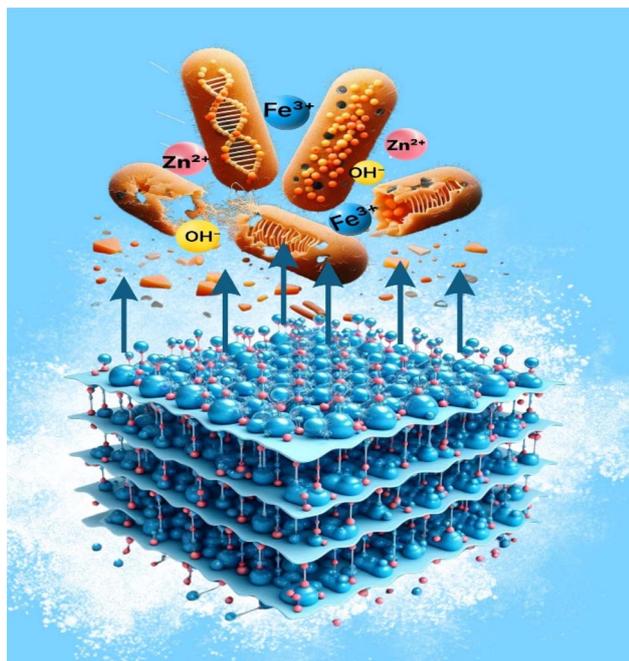### 3.8. Cost analysis of detecting for caffeine residues during adsorption study

A key aspect of performance analysis is the cost estimation of the prepared adsorbents, as cost-effective adsorbents offer significant advantages for real-life applications. For this study, the cost estimation of CaO support was conducted first. As detailed in Table S1 of the ESI,† eggshells can be considered as having a zero-acquisition cost. The equipment used, including crushers, dryers, and a calcination furnace, incurred energy costs of 1.28, 1.60, and 0.32 USD, respectively. With a yield of 25 g per batch, the total cost of CaO is approximately 0.13 USD per g. Next, the cost of LDH was estimated, as shown in Table S2 of the ESI.† Including both material and energy costs, with a yield of 4 g per batch, the overall cost is estimated to be 8.14 USD per g. For the composite material, the cost was estimated to be approximately 5.47 USD per g, as detailed in Table S3 of the ESI.†

### 3.9. *In vitro* cytotoxicity of CaO, ZnFe-LDH and CaO/ZnFe-LDH against WI-38 cell line

As illustrated in Fig. 12, the MTT assay was employed to evaluate the potential cytotoxicity of CaO, ZnFe-LDH, and CaO/ZnFe-LDH on the WI-38 cell line. These substances were administered to the cell lines at varying concentrations 12.5, 25, 50, 100, and 200 $\mu$g mL$^{-1}$ and incubated for 48 hours. Following this,

**Scheme 3** Mechanism for the antibacterial activity of the ZnFe-LDH.

**Table 6** Antimicrobial activity as MIC ($\mu g\ mL^{-1}$) of CaO, ZnFe-LDH, and CaO/ZnFe-LDH against methicillin-resistant *Staphylococcus aureus* (*MRSA*) and *Escherichia coli*

| Compounds | Gram (+) bacteria *MRSA* | Gram (−) bacteria *E.coli* |
|---|---|---|
| Standard | $0.87 \pm 0.08$ | $0.44 \pm 0.02$ |
| ZnFe-LDH | $3.5 \pm 0.6$ | $1.75 \pm 0.3$ |
| CaO NPs | $7 \pm 0.21$ | $3.5 \pm 0.15$ |
| CaO/ZnFe-LDH | $0.87 \pm 0.45$ | $0.87 \pm 0.21$ |

including Gram-positive bacteria, *MRSA*, Gram-negative bacteria, *E. coli*, using the agar disk diffusion method. Ampicillin, a reference antibiotic, was used for comparison. ZnFe-LDH, CaO, and CaO/ZnFe-LDH demonstrated significant *in vitro* antimicrobial activity against all tested microorganisms (Table 5 and Fig. 13). This activity is likely due to the release of hydroxyl ion radicals in aqueous environments (Scheme 3), which are highly reactive oxidant radicals that interact with various biomolecules. These findings are consistent with those reported by previous studies.[49] The underlying mechanism for this antibacterial activity is linked to the emission of hydroxyl ion radicals from ZnFe-LDH, CaO, and CaO/ZnFe-LDH (Scheme 4). These ions form highly reactive free radicals known to damage various critical biomolecules, including disrupting DNA, bacterial cytoplasmic membranes, and denaturing proteins.[50] Another contributing factor could be the positive charge of ZnFe-LDH, CaO, and CaO/ZnFe-LDH, which plays a significant role in their antibacterial effect. This positive charge can damage cells and lead to growth inhibition, particularly effective against the cell walls of Gram-positive bacteria. These walls are composed of peptide polyglycogen with numerous pores that allow easy entry of foreign molecules, facilitating rapid ion absorption. It is suggested that the smaller sizes of these LDH layers facilitate a more straightforward release of these damaging free radicals.[51]

Table 5 presents the antimicrobial efficacy of CaO, ZnFe-LDH, and CaO/ZnFe-LDH, showing the average zone of

the MTT assay was performed to assess cell viability. Control cells were treated only with diluent. After 48 hours of exposure to 200 $\mu g\ mL^{-1}$ of CaO, ZnFe-LDH, and CaO/ZnFe-LDH, the cell viability was found to be $70 \pm 1.5\%$, $63 \pm 1.8\%$, and $68 \pm 1\%$, respectively. These results suggest that the prepared samples exhibited minimal cytotoxic effects on the cells under the tested conditions.

### 3.10. Antibacterial activity

Given their bioremediation and biocompatibility properties, ZnFe-LDH, CaO and CaO/ZnFe-LDH have potential for use in biomedical applications. The antimicrobial activity of these compounds was explored against a variety of microorganisms,



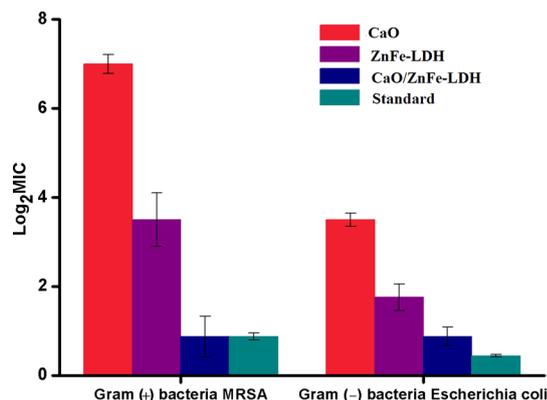**Scheme 4** Mechanism for the antibacterial activity of the CaO/ZnFe-LDH.

Fig. 14 Antimicrobial activity as MIC ($\mu$g mL$^{-1}$) of CaO, ZnFe-LDH and CaO/ZnFe-LDH against *MRSA* and *E. coli*.

Table 7 The penalty points (PPs) of the proposed method per the analytical Eco-scale

|            | Analytical Eco-scale | PPs |
|------------|----------------------|-----|
| Reagents   | Ethanol              | 1   |
|            | Sodium hydroxide     | 2   |
| Instruments | Oven                | 2   |
|            | UV-vis spectrometry  | 0   |
|            | X-ray diffractometry | 2   |
|            | Waste                | 5   |
|            | Total pp             | 12  |
|            | Eco-scale            | 88  |

inhibition in millimeters (mm) ± standard deviation, beyond the well diameter of 6 mm. This was observed across clinically relevant pathogenic microorganisms, namely *MRSA* and *E. coli*. The experiments were conducted at a concentration of 10 mg mL$^{-1}$ for the samples tested. The results are summarized in the table below.

**3.10.1. MIC values of ZnFe-LDH, CaO and CaO/ZnFe-LDH nanocomposites.** The MIC values of ZnFe-LDH, CaO, and CaO/ZnFe-LDH nanocomposites against both *MRSA* and *E. coli* microorganisms are detailed in Table 6. It is evident that the MIC values range from 0.87 to 7.00 $\mu$g mL$^{-1}$, depending on the type of microorganism. The results demonstrate strong antibacterial activity for these nanosized LDHs, as shown in Fig. 14.

### 3.11. Greenness profile of the created method

The concept of "green analytical chemistry" (GAC) encourages analytical chemists to address environmental, health, and safety considerations in their work. A method is deemed to exhibit superior green analysis if its Eco-scale score exceeds 75, with a higher score approaching 100 indicating greater environmental friendliness. A new method with an Eco-scale score of 88 represents a significant advancement in green analytical techniques. The Eco-scale score is detailed in Table 7. Additionally, AGREE is a green assessment tool that provides a quantitative score reflecting how well a methodology aligns



Fig. 15 The score of the green metric AGREE for the new method.

with the twelve key principles of green analytical chemistry. Methods that receive higher scores are considered more environmentally friendly; the total score is illustrated in the center of the circle pictogram, as shown in Fig. 15.

## 4 Conclusion

The three adsorbents—CaO, ZnFe-LDH, and CaO/ZnFe-LDH— are easy to prepare and environmentally friendly materials that effectively remove COF from water. In this study, the adsorbents were synthesized by modifying the chemical environment of metal salt solutions, and their effects on COF adsorption were assessed using single-factor analysis. During the experimental phase of wastewater treatment, the impact of initial concentration, adsorption time, material dosage, and pH on the COF adsorption rate was investigated. The maximum adsorption capacities obtained were 152.35 mg g$^{-1}$ for ZnFe-LDH and 194.87 mg g$^{-1}$ for CaO/ZnFe-LDH. The study highlights the potential of these synthesized materials as effective agents for water treatment. The MTT assay results indicated minimal toxicity, with cell viability consistently above 60%, suggesting that these materials are biocompatible and safe for various applications. Additionally, the robust antimicrobial properties of these compounds against both *E. coli* and *MRSA* were demonstrated, with MIC values ranging from 0.87 to 7 $\mu$g mL$^{-1}$, indicating effective microbial growth inhibition at relatively low concentrations. These findings support the potential use of CaO, ZnFe-LDH, and CaO/ZnFe-LDH composites in enhancing water treatment technologies, offering both safety and efficacy in microbial control. The results also open avenues for the application of these materials, either alone or in combination with other nanomaterials, to develop inorganic or synthetic nanocomposites that valorize natural waste. Such valorization supports a transition toward sustainable production and consumption, in line with circular economy principles. The study utilized the Analytical Eco-scale and the Analytical GREEnness Calculator (AGREE) as green metrics.

## Consent for publication

The authors confirm: that the work described has not been published before; that it is not under consideration for

publication elsewhere; that its publication has been approved by all co-authors.

## Ethical statement

Not applicable as the study not applied on human or animals study. The article does not include any studies on human participants or animals conducted by any of the authors.

## Data availability

The datasets used and/or analyzed during the current study available from the corresponding author on reasonable request.

## Conflicts of interest

The authors declare no competing interests.

## Acknowledgements

## References

1 H. M. Abdel-Aziz, R. S. Farag and S. A. Abdel-Gawad, Removal of caffeine from aqueous solution by green approach using Ficus Benjamina zero-valent iron/copper nanoparticles, *Adsorpt. Sci. Technol.*, 2020, **38**(9–10), 325–343, DOI: **10.1177/0263617420947495**.

2 E. N. Oliveira, *et al.*, Highly effective adsorption of caffeine by a novel activated carbon prepared from coconut leaf, *Environ. Sci. Pollut. Res.*, 2022, **29**(33), 50661–50674, DOI: **10.1007/s11356-022-18788-w.**

3 J. L. Sotelo, G. Ovejero, A. Rodríguez, S. Álvarez and J. García, Study of natural clay adsorbent sepiolite for the removal of caffeine from aqueous solutions: batch and fixed-bed column operation, *Water, Air, Soil Pollut.*, 2013, **224**(3), DOI: **10.1007/s11270-013-1466-8**.

4 I. Anastopoulos and I. Pashalidis, The application of oxidized carbon derived from Luffa cylindrica for caffeine removal. Equilibrium, thermodynamic, kinetic and

5 mechanistic analysis, *J. Mol. Liq.*, 2019, **296**, 112078, DOI: **10.1016/j.molliq.2019.112078**.

5 P. V. dos Santos Lins, D. C. Henrique, A. H. Ide, C. L. d. P. e Silva Zanta and L. Meili, Evaluation of caffeine adsorption by MgAl-LDH/biochar composite, *Environ. Sci. Pollut. Res.*, 2019, **26**(31), 31804–31811, DOI: **10.1007/s11356-019-06288-3**.

6 Y. M. Correa-Navarro, L. Giraldo and J. C. Moreno-Piraján, Biochar from fique bagasse for remotion of caffeine and diclofenac from aqueous solution, *Molecules*, 2020, **25**(8), 1–17, DOI: **10.3390/molecules25081849**.

7 K. K. Beltrame, A. L. Cazetta, P. S. C. de Souza, L. Spessato, T. L. Silva and V. C. Almeida, Adsorption of caffeine on mesoporous activated carbon fibers prepared from pineapple plant leaves, *Ecotoxicol. Environ. Saf.*, 2018, **147**(August 2017), 64–71, DOI: **10.1016/j.ecoenv.2017.08.034**.

8 S. Álvarez, R. S. Ribeiro, H. T. Gomes, J. L. Sotelo and J. García, Synthesis of carbon xerogels and their application in adsorption studies of caffeine and diclofenac as emerging contaminants, *Chem. Eng. Res. Des.*, 2015, **95**, 229–238, DOI: **10.1016/j.cherd.2014.11.001**.

9 R. K. Mahmoud, M. Taha, A. Zaher and R. M. Amin, Understanding the physicochemical properties of Zn–Fe LDH nanostructure as sorbent material for removing of anionic and cationic dyes mixture, *Sci. Rep.*, 2021, **11**(1), 1–19, DOI: **10.1038/s41598-021-00437-w**.

10 K. Delhiraja, K. Vellingiri, D. W. Boukhvalov and L. Philip, Development of Highly Water Stable Graphene Oxide-Based Composites for the Removal of Pharmaceuticals and Personal Care Products, *Ind. Eng. Chem. Res.*, 2019, **58**(8), 2899–2913, DOI: **10.1021/acs.iecr.8b02668**.

11 N. Laohavisuti, B. Boonchom, W. Boonmee, K. Chaiseeda and S. Seesanong, Simple recycling of biowaste eggshells to various calcium phosphates for specific industries, *Sci. Rep.*, 2021, **11**(1), 1–11, DOI: **10.1038/s41598-021-94643-1**.

12 M. H. Azarian and W. Sutapun, Biogenic calcium carbonate derived from waste shells for advanced material applications: a review, *Front. Mater.*, 2022, **9**(November), 1–17, DOI: **10.3389/fmats.2022.1024977**.

13 A. Hart, Mini-review of waste shell-derived materials' applications, *Waste Manag. Res.*, 2020, **38**(5), 514–527, DOI: **10.1177/0734242X19897812**.

14 S. A. Bhawani, S. S. Fong and M. N. M. Ibrahim, Spectrophotometric Analysis of Caffeine, *Int. J. Anal. Chem.*, 2015, **2015**, DOI: **10.1155/2015/170239**.

15 A. Gałuszka, Z. Migaszewski and J. Namieśnik, The 12 principles of green analytical chemistry and the significance mnemonic of green analytical practices, *TrAC, Trends Anal. Chem.*, 2013, **50**, 78–84, DOI: **10.1016/j.trac.2013.04.010**.

16 E. Y. Santali, *et al.*, Greenness Assessment of Chromatographic Methods Used for Analysis of Empagliflozin: A Comparative Study, *Separations*, 2022, **9**(10), DOI: **10.3390/separations9100275**.

17 F. Pena-Pereira, W. Wojnowski and M. Tobiszewski, AGREE - Analytical GREEnness Metric Approach and Software, *Anal. Chem.*, 2020, **92**(14), 10076–10082, DOI: **10.1021/acs.analchem.0c01887**.

18 A. Gałuszka, Z. M. Migaszewski, P. Konieczka and J. Namieśnik, Analytical Eco-Scale for assessing the greenness of analytical procedures, *TrAC, Trends Anal. Chem.*, 2012, **37**, 61–72, DOI: **10.1016/j.trac.2012.03.013**.

19 J. Płotka-Wasylka, A new tool for the evaluation of the analytical procedure: green analytical procedure index, *Talanta*, 2018, **181**, 204–209, DOI: **10.1016/j.talanta.2018.01.013**.

20 Q. Wang, *et al.*, As(III) removal from wastewater and direct stabilization by in situ formation of Zn-Fe layered double hydroxides, *J. Hazard. Mater.*, 2021, **403**(September 2020), 123920, DOI: **10.1016/j.jhazmat.2020.123920**.

21 O. Koba-Ucun, *et al.*, Toxicity of zn-fe layered double hydroxide to different organisms in the aquatic environment, *Molecules*, 2021, **26**(2), 1–14, DOI: **10.3390/molecules26020395**.

22 A. Zaher, M. Taha, A. A. Farghali and R. K. Mahmoud, Zn/Fe LDH as a clay-like adsorbent for the removal of oxytetracycline from water: combining experimental results and molecular simulations to understand the removal mechanism, *Environ. Sci. Pollut. Res.*, 2020, **27**(11), 12256–12269, DOI: **10.1007/s11356-020-07750-3**.

23 C. Li, G. Zhao, L. Liu, J. Yu, X. Jiang and F. Jiao, Preparation of CuOx@ZnFe-LDH composites and photocatalytic degradation of 4-nitrophenol by activated persulfate, *J. Mater. Sci.: Mater. Electron.*, 2018, **29**(22), 19461–19471, DOI: **10.1007/s10854-018-0076-z**.

24 Y. Wang, S. Zhou, G. Zhao, C. Li, L. Liu and F. Jiao, Fabrication of SnWO4/ZnFe-layered double hydroxide composites with enhanced photocatalytic degradation of methyl orange, *J. Mater. Sci.: Mater. Electron.*, 2020, **31**(15), 12269–12281, DOI: **10.1007/s10854-020-03772-2**.

25 J. Jitjamnong, A. Luengnaruemitchai, N. Samanwonga and N. Chuaykarn, Biodiesel production from canola oil and methanol using ba impregnated calcium oxide with microwave irradiation-assistance, *Chiang Mai J. Sci.*, 2019, **46**(5), 987–1000.

26 Y. Y. Margaretha, H. S. Prastyo, A. Ayucitra and S. Ismadji, Calcium oxide from pomacea sp. shell as a catalyst for biodiesel production, *Int. J. Energy Environ. Eng.*, 2012, **3**(1), 1–9, DOI: **10.1186/2251-6832-3-33**.

27 B. Barrocas, A. J. Silvestre, A. G. Rolo and O. C. Monteiro, The effect of ionic Co presence on the structural, optical and photocatalytic properties of modified cobalt-titanate nanotubes, *Phys. Chem. Chem. Phys.*, 2016, **18**(27), 18081–18093, DOI: **10.1039/c6cp01889k**.

28 B. Barrocas, M. C. Neves, M. C. Oliveira and O. C. Monteiro, Enhanced photocatalytic degradation of psychoactive substances using amine-modified elongated titanate nanostructures, *Environ. Sci.: Nano*, 2018, **5**(2), 350–361, DOI: **10.1039/c7en00882a**.

29 D. C. Coelho, *et al.*, Effect of the active metal on the catalytic activity of the titanate nanotubes for dry reforming of methane, *Chem. Eng. J.*, 2016, **290**, 438–453, DOI: **10.1016/j.cej.2016.01.051**.

30 I. Saad, M. F. Eissa and R. M. Amin, Evolution and reduction reactions, *RSC Adv.*, 2024, 27488–27503, DOI: **10.1039/D4RA04105D**.

31 S. Li, *et al.*, Synthesis of layered double hydroxides from eggshells, *Mater. Chem. Phys.*, 2012, **132**(1), 39–43, DOI: **10.1016/j.matchemphys.2011.10.049**.

32 V. Vinila and J. Isac, *Synthesis and structural studies of superconducting perovskite GdBa2Ca3Cu4O10.5+δ nanosystems*, 2022, pp. 319–341, DOI: **10.1016/B978-0-12-820558-7.00022-4**.

33 H. A. Younes, *et al.*, Computational and experimental studies on the efficient removal of diclofenac from water using ZnFe-layered double hydroxide as an environmentally benign absorbent, *J. Taiwan Inst. Chem. Eng.*, 2019, **102**, 297–311, DOI: **10.1016/j.jtice.2019.06.018**.

34 M. A. A. Aziz, S. Triwahyono, A. A. Jalil, H. A. A. Rapaib and A. E. Atabani, Transesterification of moringa oleifera oil to biodiesel using potassium flouride loaded eggshell as catalyst, *Malay. J. Catal.*, 2016, **1**, 22–26.

35 S. L. Hsieh, *et al.*, CaO recovered from eggshell waste as a potential adsorbent for greenhouse gas CO2, *J. Environ. Manage.*, 2021, **297**, DOI: **10.1016/j.jenvman.2021.113430**.

36 M. D. Putra, Y. Ristianingsih, R. Jelita, C. Irawan and I. F. Nata, Potential waste from palm empty fruit bunches and eggshells as a heterogeneous catalyst for biodiesel production, *RSC Adv.*, 2017, **7**(87), 55547–55554, DOI: **10.1039/c7ra11031f**.

37 G. V. Sree, P. Nagaraaj, K. Kalanidhi, C. A. Aswathy and P. Rajasekaran, Calcium oxide a sustainable photocatalyst derived from eggshell for efficient photo-degradation of organic pollutants, *J. Clean. Prod.*, 2020, **270**, 122294, DOI: **10.1016/j.jclepro.2020.122294**.

38 T. T. Win and M. M. Khine, Synthesis and Characterization of CaO and KF Doped CaO (KF/CaO) Derived from Chicken Eggshell Waste as Heterogeneous Catalyst in Biodiesel Production, *Technol. Sci. Am. Sci. Res. J. Eng.*, 2017, **38**(2), 134–151, available, **https://asrjetsjournal.org/**.

39 M. Minakshi, S. Higley, C. Baur, D. R. G. Mitchell, R. T. Jones and M. Fichtner, Calcined chicken eggshell electrode for battery and supercapacitor applications, *RSC Adv.*, 2019, **9**(46), 26981–26995, DOI: **10.1039/c9ra04289j**.

40 Z. Li, *et al.*, Efficient solid base derived from eggshell for heterogeneous biodiesel production, *Indian J. Biochem. Biophys.*, 2021, **58**(5), 457–463, DOI: **10.56042/ijbb.v58i5.55390**.

41 S. Mallakpour, Z. Radfar and M. Feiz, Chitosan/tannic acid/ZnFe layered double hydroxides and mixed metal oxides nanocomposite for the adsorption of reactive dyes, *Carbohydr. Polym.*, 2023, **305**(October 2022), 120528, DOI: **10.1016/j.carbpol.2022.120528**.

42 D. Bharali, S. Saikia, R. Devi, B. M. Choudary, N. K. Gour and R. C. Deka, Photocatalytic degradation of phenol and its derivatives over ZnFe layered double hydroxide, *J. Photochem. Photobiol., A*, 2023, **438**, 114509.

43 A. Elhalil, *et al.*, Enhanced photocatalytic degradation of caffeine as a model pharmaceutical pollutant by Ag-ZnO-

Al2O3 nanocomposite, *Desalin. Water Treat.*, 2017, **94**(January), 254–262, DOI: **10.5004/dwt.2017.21587**.

44 M. Harja and G. Ciobanu, Studies on adsorption of oxytetracycline from aqueous solutions onto hydroxyapatite, *Sci. Total Environ.*, 2018, **628–629**, 36–43, DOI: **10.1016/j.scitotenv.2018.02.027**.

45 M. Brdar, M. Šćiban, A. Takači and T. Došenović, Comparison of two and three parameters adsorption isotherm for Cr(VI) onto Kraft lignin, *Chem. Eng. J.*, 2012, **183**(February), 108–111, DOI: **10.1016/j.cej.2011.12.036**.

46 S. Kaur, S. Rani and R. K. Mahajan, Congo Red Biowaste Materials as Adsorbents, *J. Chem.*, 2012, **2013**, 12.

47 A. S. Al-Gorair, Treatment of wastewater from cationic dye using eco-friendly nanocomposite: characterization, adsorption and kinetic studies, *Egypt. J. Aquat. Res.*, 2019, **45**(1), 25–31, DOI: **10.1016/j.ejar.2018.10.004**.

48 S. Sun, E. Yu, R. Hu, Y. Li and Z. Wei, Synthesis and study of poly (phthalic anhydride-β-cyclodextrin) for the efficient adsorption of cationic dyes from industrial wastewater, *Chem. Eng. Res. Des.*, 2023, **194**, DOI: **10.1016/j.cherd.2023.05.025**.

49 J. Awassa, D. Cornu, S. Soulé, C. Carteret, C. Ruby and S. El-Kirat-Chatel, Divalent metal release and antimicrobial effects of layered double hydroxides, *Appl. Clay Sci.*, 2022, 106369.

50 J. Chaudhary, G. Tailor, B. Yadav and O. Michael, Synthesis and biological function of Nickel and Copper nanoparticles, *Heliyon*, 2019, **5**, e01878, DOI: **10.1016/j.heliyon.2019.e01878**.

51 S. A. Aziz, Y. Gadelhak, M. Mohamed and R. Mahmoud, Antimicrobial properties of promising Zn–Fe based layered double hydroxides for the disinfection of real dairy wastewater effluents, *Sci. Rep.*, 2023, **13**, DOI: **10.1038/s41598-023-34488-y**.